# Pulsars:

## a tool for test of theories of gravity

Jérôme Pétri

Observatoire Astronomique de Strasbourg
Université de Strasbourg

31/5/2013

# Outline



# The discovery in 1967: a revolution in astrophysics

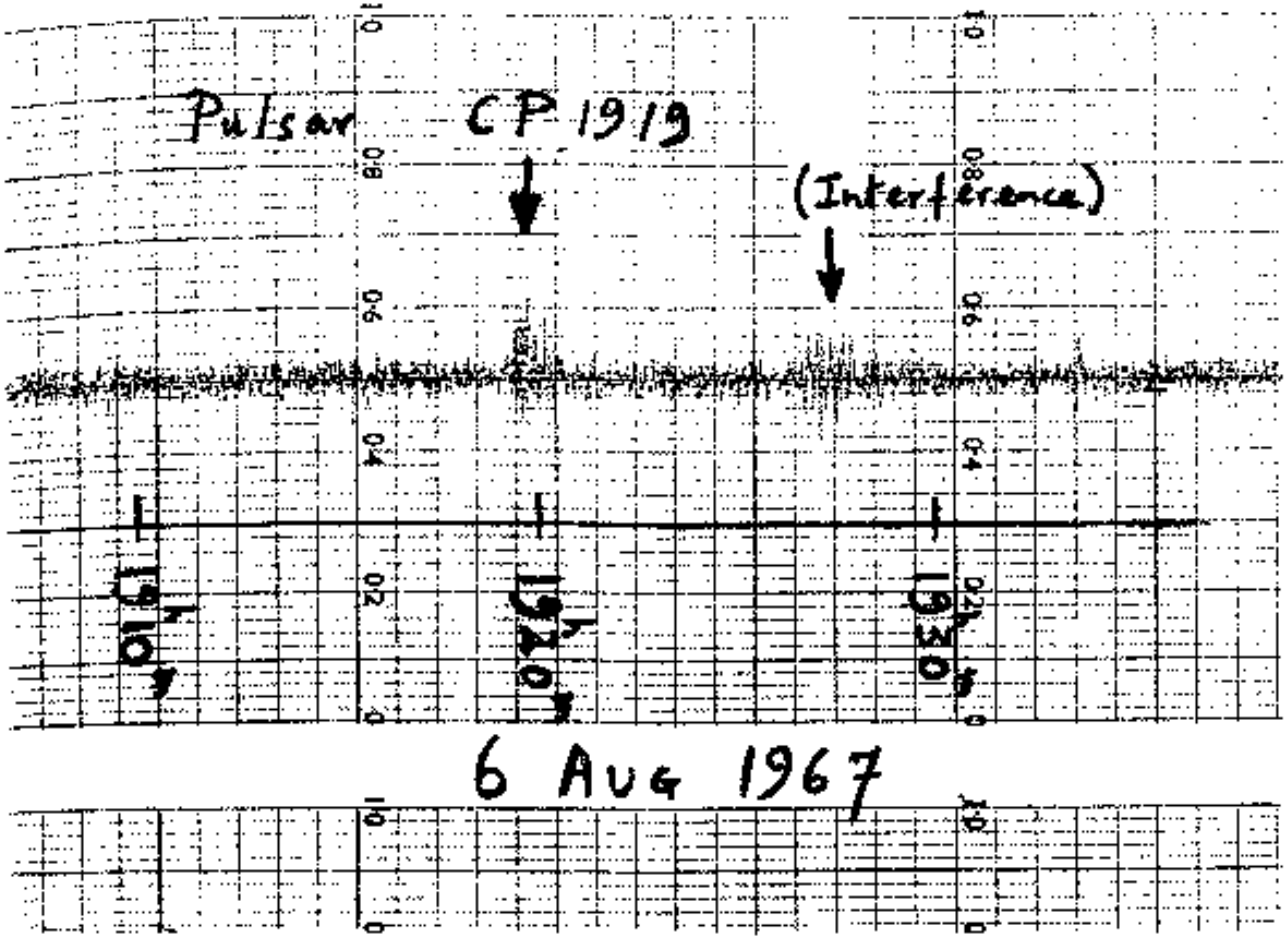

# Pulsar magnetosphere: general picture

What is a pulsar?

# Pulsar magnetosphere: general picture

What is a pulsar?

1. neutron star
   compact object $\Rightarrow$ strong gravity effects

# Pulsar magnetosphere: general picture

What is a pulsar?

1. neutron star
   compact object $\Rightarrow$ strong gravity effects
2. strongly magnetized
   $\Rightarrow$ plasmas, QED effects (pair creation)

# Pulsar magnetosphere: general picture

What is a pulsar?

1. neutron star
   compact object $\Rightarrow$ strong gravity effects
2. strongly magnetized
   $\Rightarrow$ plasmas, QED effects (pair creation)
3. rotating
   $\Rightarrow$ huge electric fields

# Pulsar magnetosphere: general picture

## What is a pulsar?

1. neutron star
   compact object $\Rightarrow$ strong gravity effects
2. strongly magnetized
   $\Rightarrow$ plasmas, QED effects (pair creation)
3. rotating
   $\Rightarrow$ huge electric fields

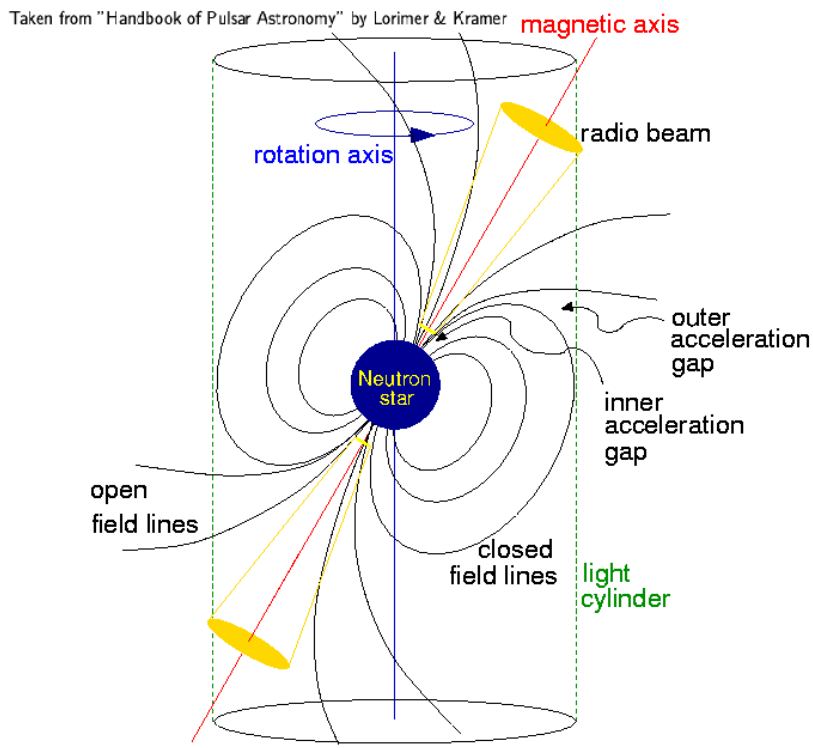


Credit: A.K. Harding

# Pulsar magnetosphere: general picture

## What is a pulsar?

1. neutron star
   compact object $\Rightarrow$ strong gravity effects
2. strongly magnetized
   $\Rightarrow$ plasmas, QED effects (pair creation)
3. rotating
   $\Rightarrow$ huge electric fields

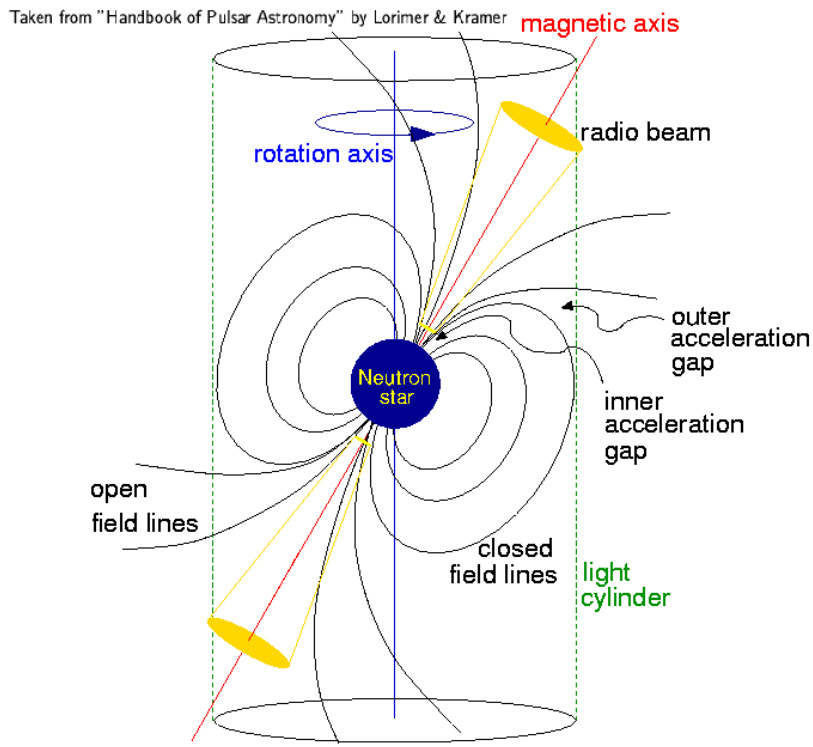


Credit: A.K. Harding

## Some useful definitions

- obliquity $\chi$: angle between magnetic moment $\vec{\mu}$ and rotation axis $\vec{\Omega}$
- aligned/perpendicular/oblique rotator: $\chi = 0/90^o/$any value
- light cylinder radius: surface on which a particle corotating with the neutron star reaches the speed of light $c$: $r_{\rm L} = c/\Omega$
  $\Rightarrow$ transition from quasi-static to wave zone

# Neutron stars main classes

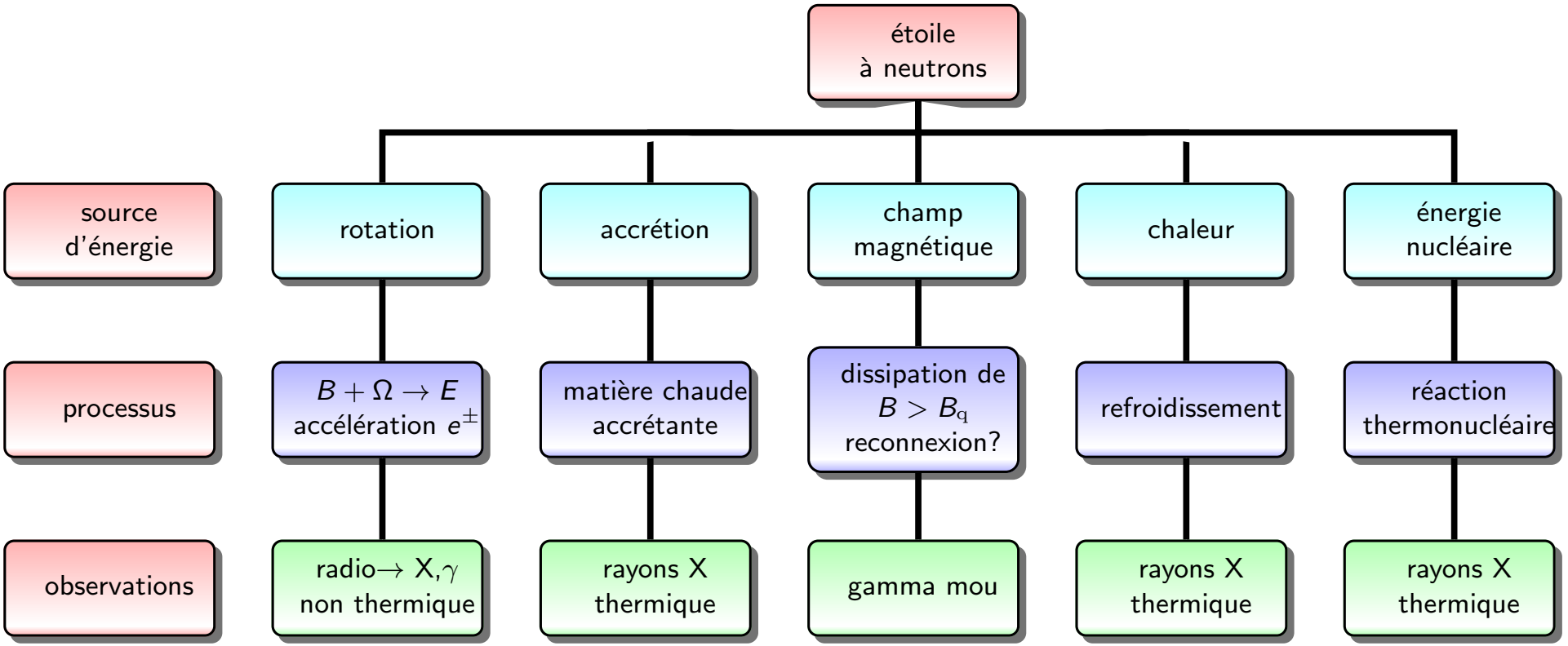


Figure: Les différentes classes de pulsars dont la distinction se fait par la source d'énergie à l'origine de l'activité de l'étoile à neutrons.

# Pulsar magnetosphere: orders of magnitude

From observations

- period $P \in [1\ ms, 1\ s]$
- period derivative $\dot{P} \in [10^{-18}, 10^{-15}]$
- spin-down losses well constrained

$$L_{\rm sp} = 4\,\pi^2\,I\,\dot{P}\,P^{-3} \approx 10^{24-31}\ W$$

very different from black holes or accreting neutron stars

- inferred magnetic field estimate by dipole radiation

$$B = 3.2 \times 10^{15}\,\sqrt{P\,\dot{P}} = 10^{5-8}\ T$$

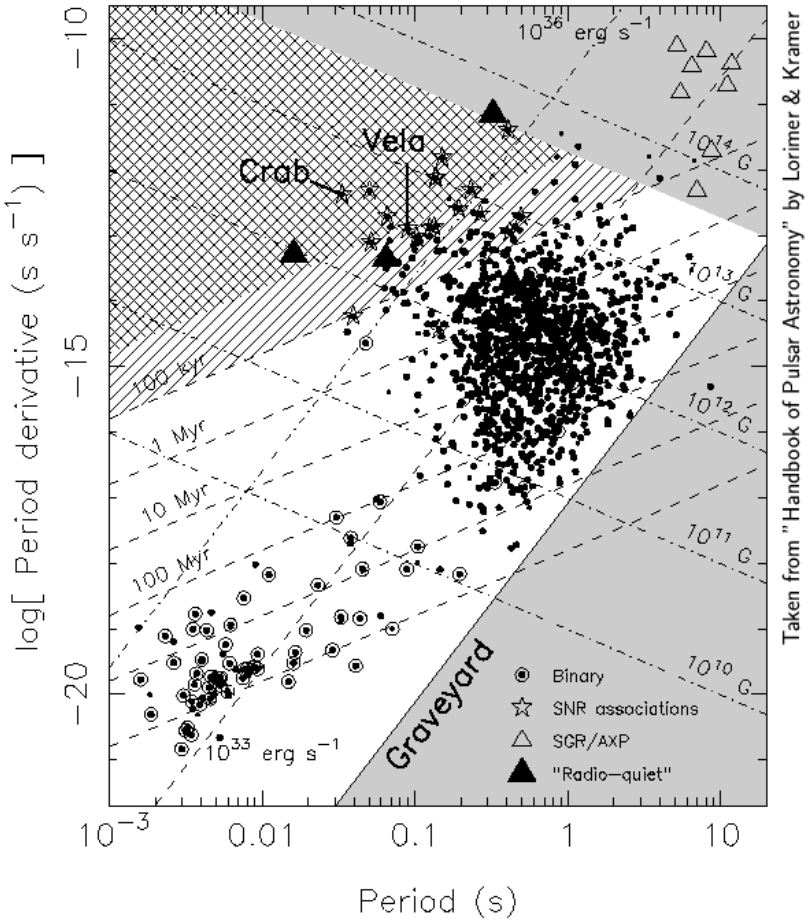


Credit: Lorimer & Kramer

# Pulsar magnetosphere: orders of magnitude

## Electromagnetic and gravitational field characteristics

- electric field induced at the stellar crust

$$E = \Omega\, B\, R = 10^{13}\ \mathrm{V/m}$$

  $\Rightarrow$ instantaneous acceleration at ultra-relativistic speeds, Lorentz factor $\gamma \gg 1$ ($\tau_{\mathrm{acc}} < 10^{-20}$ s)

- negligible gravitational force !!!

$$\frac{F_{\mathrm{grav}}}{F_{\mathrm{em}}} \approx \frac{G\, M\, m_p / R^2}{e\, \Omega\, B\, R} \approx 10^{-12} \ll 1 \qquad (1)$$

even smaller for electrons/positrons ($m_e/m_p$)
$\Rightarrow$ dynamic of the magnetosphere dominated by the electromagnetic field

## Neutron star characteristics

- masse $M \approx 1.4\, M_\odot$.
- radius $R \approx 10$ km.
- centrale density $\rho_{\mathrm{c}} \approx 10^{17}\ \mathrm{kg/m^3}$.

# The radio pulses

Difficult to summarize all observations and behaviours

## Observations

- individual observation of pulses impossible (except for rare cases).
- very strong variability of individual pulses.
- but mean (averaged/integrated) profile extremely stable.

$\Rightarrow$ average over several hundredth of periods.

$\Rightarrow$ signature unique to each pulsar (its fingerprint).

## In a pictural way

- mean profile = climate
- one pulse = weather

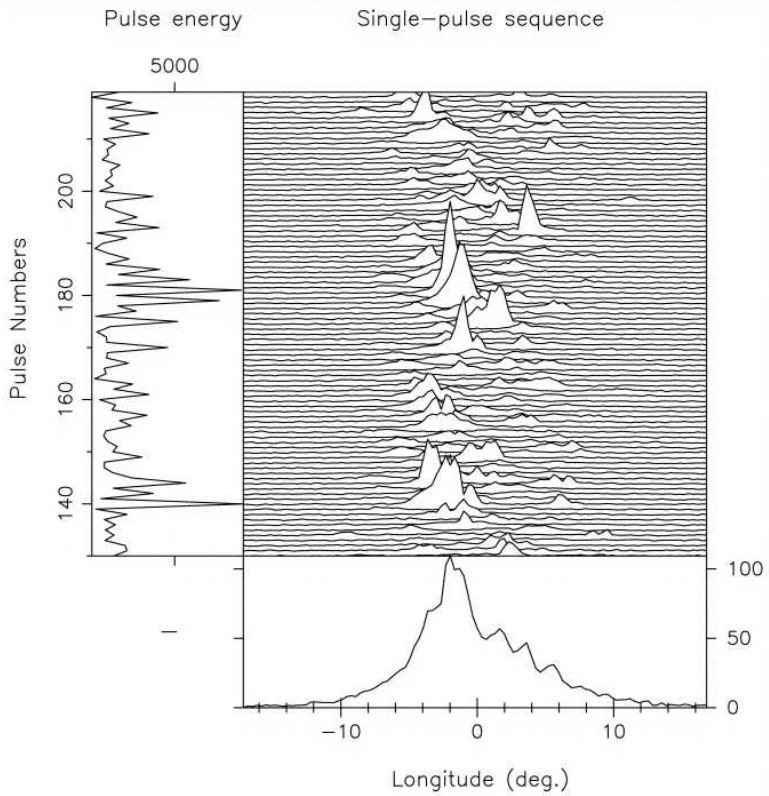


Figure: Mean profile and individual pulses of PSR B0943+10 (Deshpande ApJ, 1999)

# Width of mean profiles

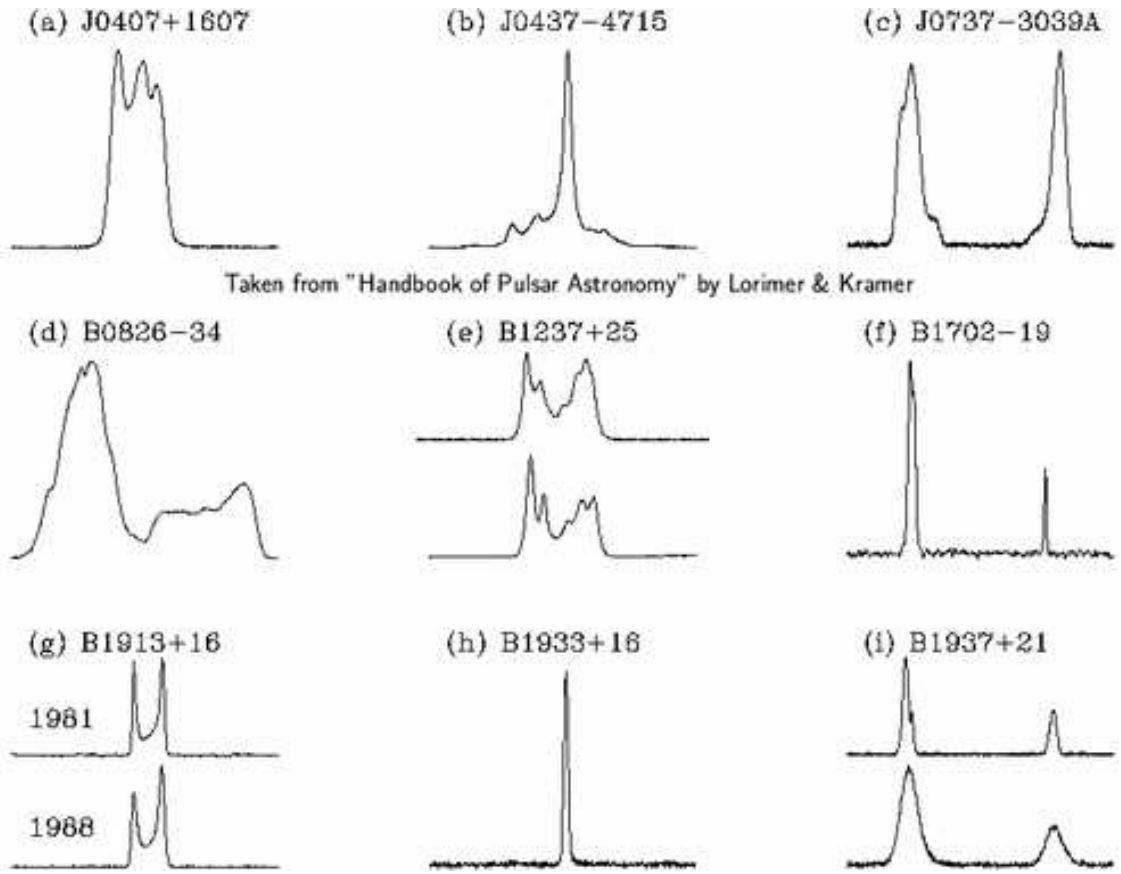


Figure: A sample of mean profiles (Lorimer & Kramer)

- duty cycle roughly constant at a few % level.
- slight variation with period.
- phenomenology more complicated for millisecond pulsars.

# Radio polarisation

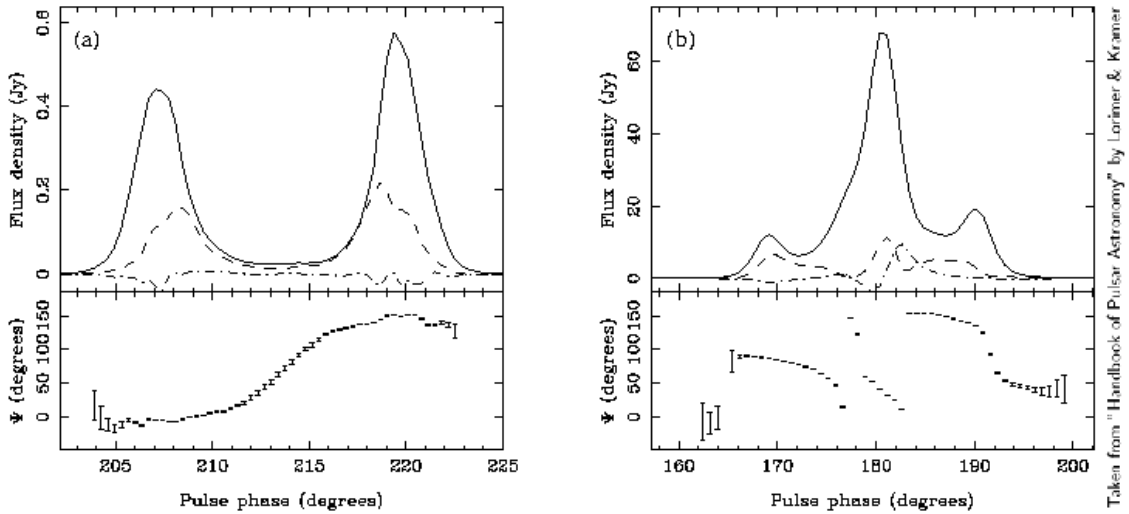


Figure: Examples of polarisation measurements (Lorimer & Kramer)

- linear and circular component.
- strong linear polarisation close to 100%.
- evolution of the polarisation with pulse phase and frequency $\Rightarrow$ indication on the geometry, the magnetic field and altitude of emission sites.
- smooth variation of polarisation angle in a S shape independant of frequency.

$\Rightarrow$ polarisation vector follows the geometry of the magnetic field lines.

$\Rightarrow$ favors the rotating vector model (but some exceptions)

# Gamma-ray pulsars: the Fermi/LAT contribution

- more than 120 gamma-ray pulsars known so far
  (a) young and energetic, visible in the whole electromagnetic spectrum (Crab).
  (b) young and radio-quiet (Geminga).
  (c) old (millisecond).
- light-curves are usually double peaked (75%), separated by 0.3 in phase.
- flux above 100 MeV is about $dN/dE \approx 10^{-8}\ \mathrm{ph/cm^2/s}$.
- mean spectra (integrated over the period) described by a power-law with exponential cut-off

$$\frac{dN}{dE} \propto E^{-\Gamma}\, e^{-E/E_\mathrm{c}} \tag{2}$$

  $\Gamma \approx 1-2$ whereas cut-off $E_\mathrm{cut} \approx 1-5$ GeV.
- spindown luminosity over many decades, $L_\mathrm{rot} \approx 10^{26} - 10^{31}$ W.
- gamma-ray luminosity $L_\gamma$ between 0.1% and almost 100% of $L_\mathrm{rot}$
  $\Rightarrow$ all the reservoir of energy converted into photons !
- cut-off gives hints on the sites of production of radiation.

(Abdo et al, ApJS, 2009, update by The Fermi-LAT collaboration, arXiv:1305.4385)

# Gamma-ray pulsars: examples

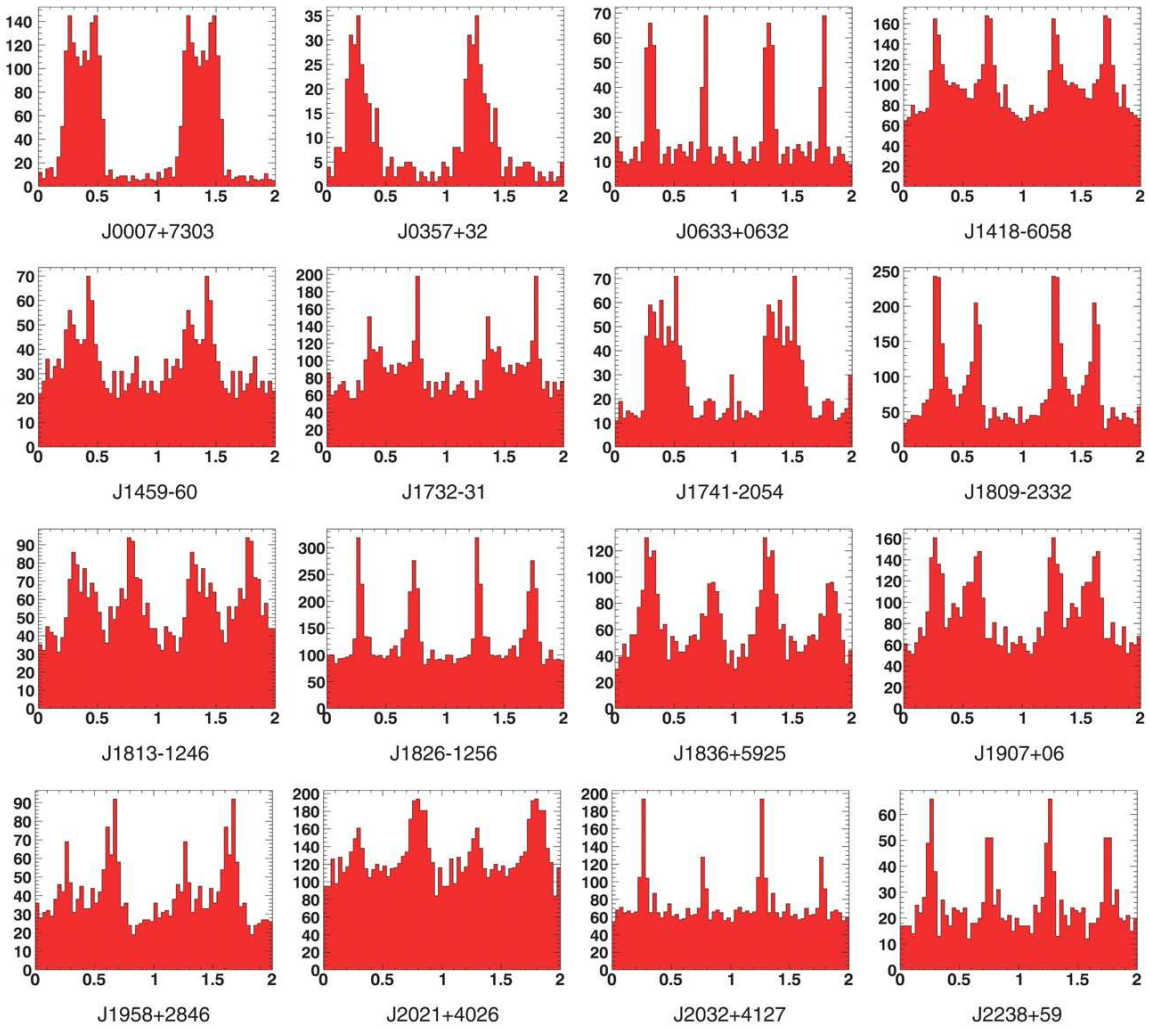


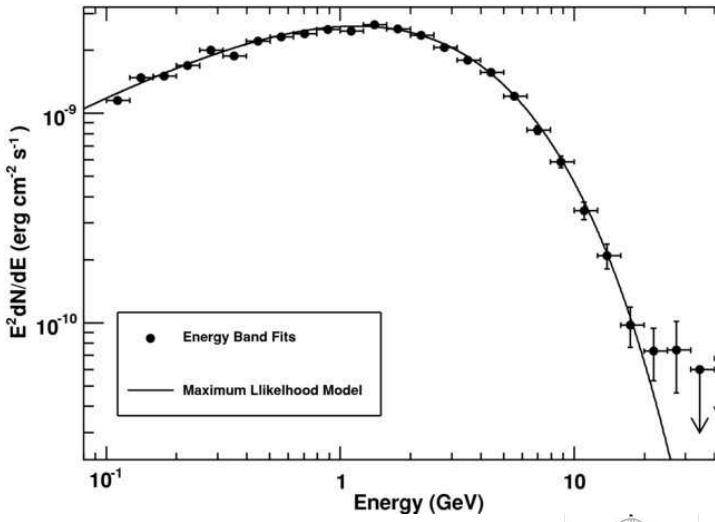


Figure: Light-curves of some gamma-ray pulsars, left, (Abdo et al, Science 2009) and Vela mean spectrum, right (Abdo et al, 2010).

# Towards very high-energies $\geq$100 GeV

- detection of pulsed emission from the Crab at 200-400 GeV
- compatible with the spectrun in the Fermi band
- spectrum as a broken power low rather exponential cut-off

$\Rightarrow$ kills all existing magnetospheric emission models !

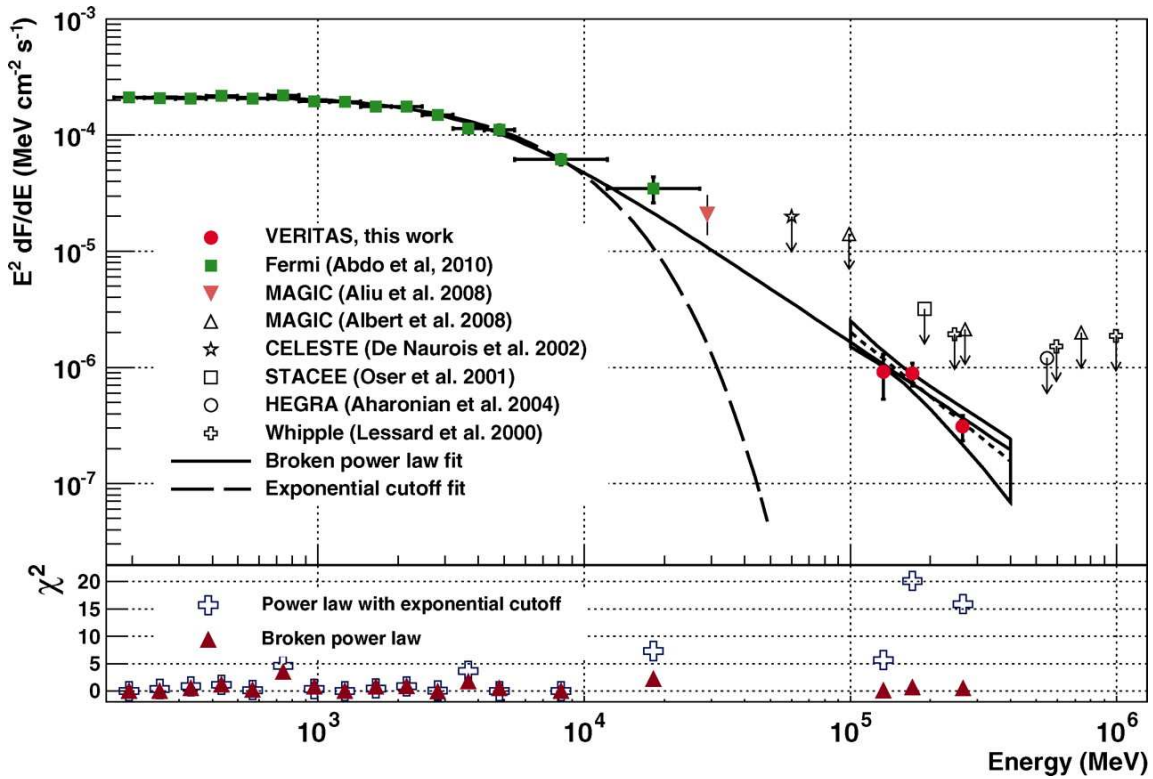


(McCann et al, ICRC 2011)

# The "standard model" of a pulsar

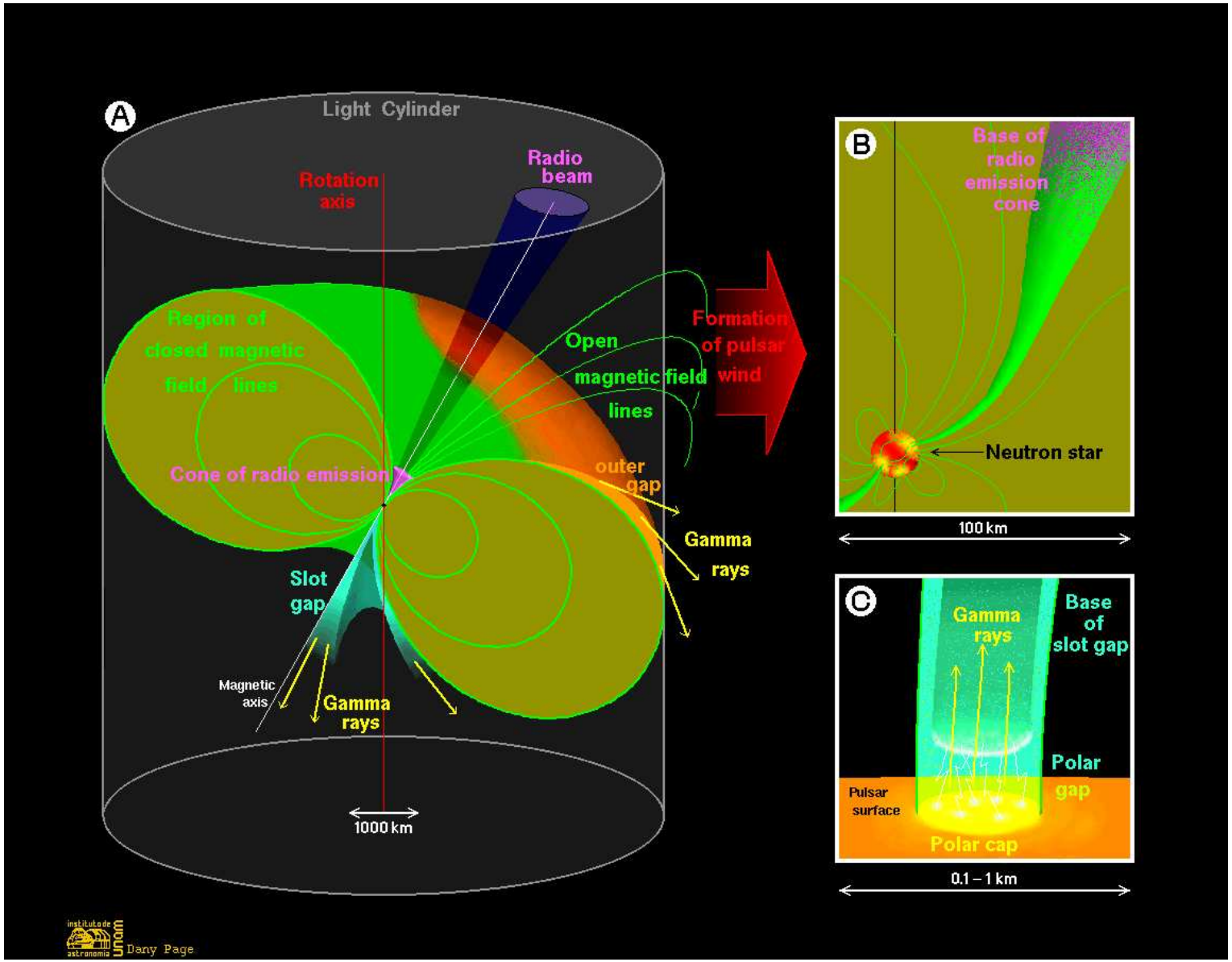

# The "standard model" of a pulsar

Basic underlying assumption: force-free magnetosphere

$$\rho_e \vec{E} + \vec{j} \wedge \vec{B} = \vec{0}$$

magnetic energy density $\frac{B^2}{2\,\mu_0} \gg$ any other energy densities

- particle inertia neglected: zero mass limit.
- no dissipation: ideal MHD

$$\vec{E} + \vec{v} \wedge \vec{B} = \vec{0}$$

- no pressure: cold plasma.

Two interpretations

- charge-separated plasma $\Rightarrow$ low particle density.
- MHD model $\Rightarrow$ quasi-neutral plasma, high particle density.

Who is right? PWN will give some clues.

A problem

$\Rightarrow$ the total charge of the system is not conserved.

$\Rightarrow$ total electric current does not vanish!

# Force-free magnetosphere

## Perpendicular rotator

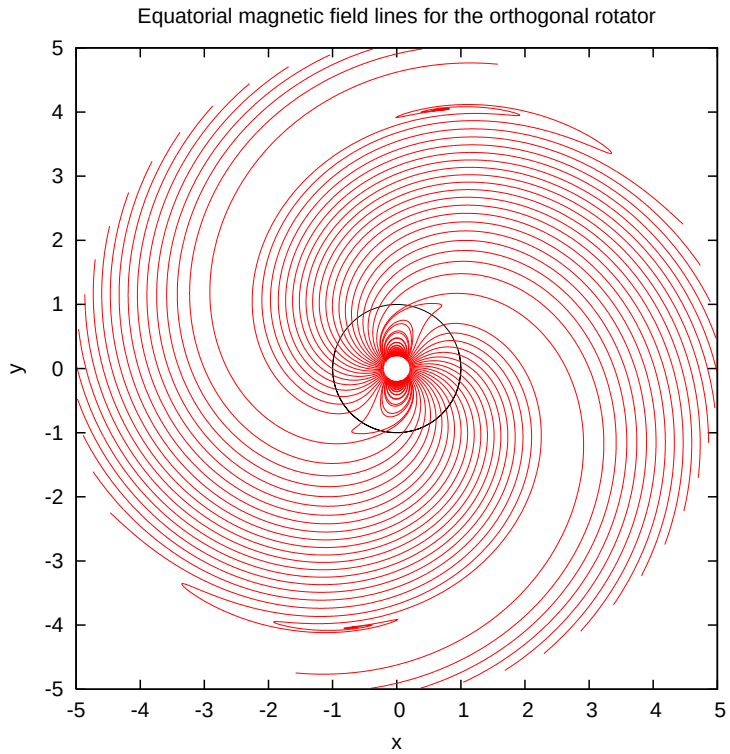


## Spin-down luminosity

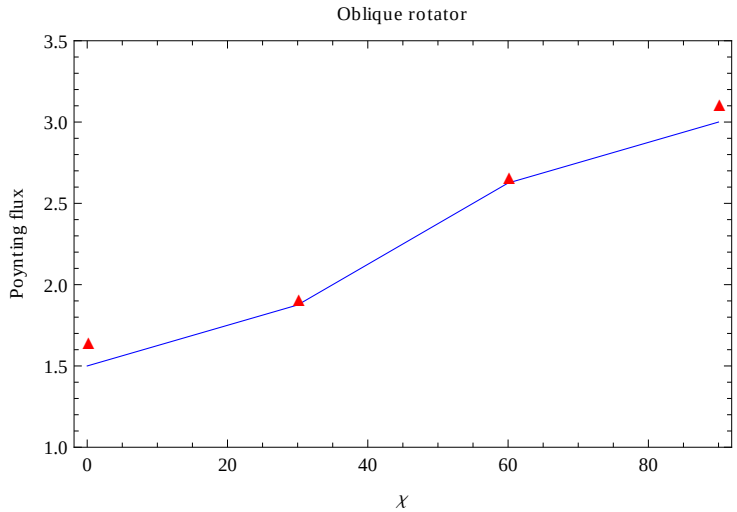


$$L_{\rm sp}^{\rm ffe} \approx \frac{3}{2} L_{\rm dip}^{\perp} (1 + \sin^2 \chi) \qquad (3a)$$

$\Rightarrow$ more realistic formula than the magnetodipole in vacuum

$$L_{\rm sp}^{\rm vac} \approx L_{\rm dip}^{\perp} \sin^2 \chi \qquad (4a)$$

$\Rightarrow$ $B_\perp$ AND $B_\parallel$ constrained.

(Pétri, MNRAS, 2012a)

# General-relativistic effects

Space-time curvature and frame dragging modify the structure of the electromagnetic field close to the neutron star surface

- amplification of the intensity of the electric field in the neighborhood of the stellar surface because of the gravitational field (Schwarzschild metric, static diagonal part).
- appearance of a longitudinal electric field (along $\vec{B}$) by Lense-Thirring effect (Kerr black hole, off diagonal elements of the metric).

(Muslimov & Tsygan, 1992)

Consequences on the magnetosphere

Quantitative modifications of

- the geometry of the polar caps, opening angle.
- the shape of the radio pulses.
- the modulation of the light-curves in X-rays for accreting pulsars.

# Emission processes: incoherent radiation

- curvature radiation: a charged particle accelerated along a curved magnetic path will radiate (obliged to follow magnetic field lines).
- cyclotron emission: a charged particle evolving non-relativistically in a magnetic field (special case of curvature radiation for a circular trajectory).
- synchrotron emission: when the same charged particle reaches relativistic speeds, foward beaming of radiation $\Rightarrow$ transition from cyclotron to synchrotron.
- inverse Compton scattering(IC): relativistic leptons scattering photons
  - thermal photons from the (X-rays).
  - photons from the surrounding nebula.
  - photons from a companion (if binary).
  - cosmic microwave background.
- synchroton-sef Compton emission(SSC): IC of the synchrotron photons produced by the leptons themselves.

BUT does not explain the radio which is peculiar because it is coherent
$\Rightarrow$ need for a coherent emission mechanism.

# Emission processes: coherent radiation

Some candidates are

- antenna: beam of particles with dispersion in velocity negligible and radiate in phase curvature radiation by a coherent beam for example
  $\Rightarrow$ difficult to set up because beam must be thin and coherence destroyed quickly.
- plasma instability: weak dispersion in velocity, particles in phase with increasing perturbation, two-stream for instance.
- maser effect with negative absorption: population inversion in the Landau levels.

No agreement yet on the processes really at work in the magnetosphere.

# Polar cap

## Main ingredients for the recipe

- polar cap size

$$R_{\rm pc} \approx R \sqrt{\frac{R}{r_L}} \approx 145 \left(\frac{P}{1\ {\rm s}}\right)^{-1/2} \ {\rm m}$$

- potential drop between centre and border of a polar cap

$$\Delta\phi = \frac{\Omega^2\, B\, R^3}{c} \approx 1.3{\times}10^{13}\ {\rm V} \left(\frac{P}{1\ s}\right)^{-2} \left(\frac{B}{10^8\ {\rm T}}\right) \left(\frac{R}{10\ {\rm km}}\right)^3$$

- particle flux from one polar cap

$$\dot{N}_{\rm pc} = 2\,\pi\, \frac{\varepsilon_0\, \Omega^2\, B\, R^3}{e} \approx 1.37{\times}10^{30}\ {\rm s}^{-1} \left(\frac{P}{1\ s}\right)^{-2} \left(\frac{B}{10^8\ {\rm T}}\right) \left(\frac{R}{10\ {\rm km}}\right)^3$$

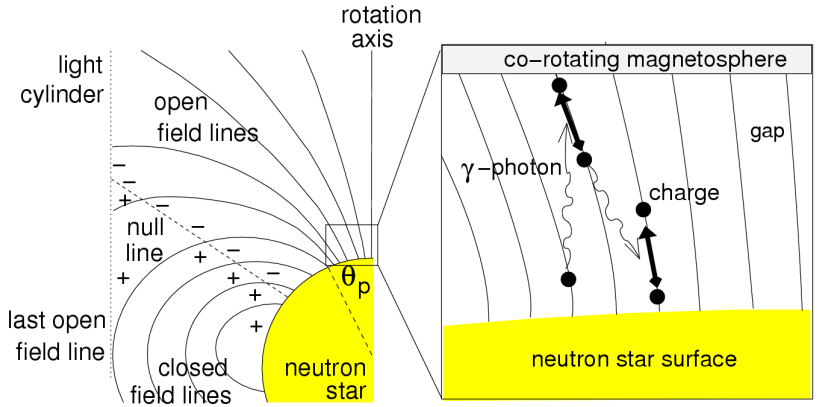


Credit: Lorimer & Kramer

## Drawbacks

- high gamma-ray opacity due to magnetic field

Sturrock (1971), Ruderman & Sutherland (1975)

# Polar cap

## Main ingredients for the recipe

- polar cap size

$$R_{\rm pc} \approx R \sqrt{\frac{R}{r_L}} \approx 145 \left(\frac{P}{1\ {\rm s}}\right)^{-1/2} \ {\rm m}$$

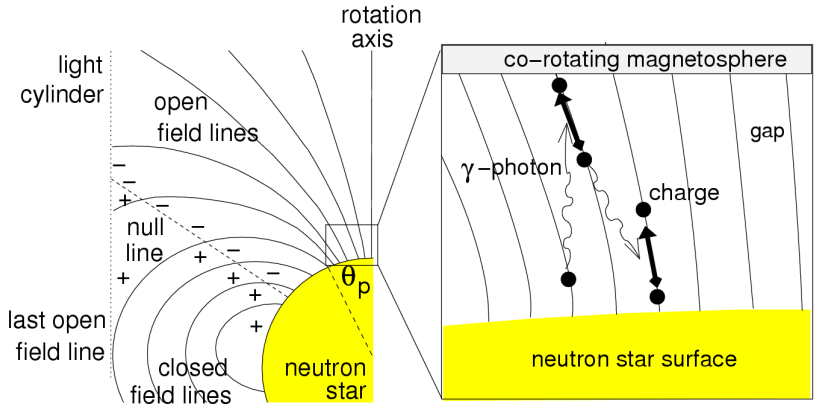


Credit: Lorimer & Kramer

- potential drop between centre and border of a polar cap

$$\Delta\phi = \frac{\Omega^2\, B\, R^3}{c} \approx 1.3{\times}10^{13}\ {\rm V} \left(\frac{P}{1\ s}\right)^{-2} \left(\frac{B}{10^8\ {\rm T}}\right) \left(\frac{R}{10\ {\rm km}}\right)^3$$

- particle flux from one polar cap

$$\dot{N}_{\rm pc} = 2\,\pi\, \frac{\varepsilon_0\, \Omega^2\, B\, R^3}{e} \approx 1.37{\times}10^{30}\ {\rm s}^{-1} \left(\frac{P}{1\ s}\right)^{-2} \left(\frac{B}{10^8\ {\rm T}}\right) \left(\frac{R}{10\ {\rm km}}\right)^3$$

## Drawbacks

- high gamma-ray opacity due to magnetic field

Sturrock (1971), Ruderman & Sutherland (1975)

$\Rightarrow$ particle outflow generating a poynting dominated wind

# Outer gap

## Another recipe

- vacuum gaps form along the null surface (where charge density vanishes $\rho_e = 0$)
- particles escape across the light-cylinder
- no replenishment from the polar cap because opposite sign of charge
- depletion regions built up accelerating electric field $E_{\parallel} \neq 0$
- particle acceleration to high Lorentz factor limited by curvature radiation reaction

Cheng, Ho & Ruderman (1986)

## Advantages

- sharp gamma-ray emission along separatrix
- geometry well constrained

## Drawbacks

- keep $\rho_e \neq \rho_{\rm GJ}$
- $e^{\pm}$ pairs return to polar cap
  $\Rightarrow$ not really interesting for feeding the wind
  $\Rightarrow$ significant polar cap heating, thermal emission to high

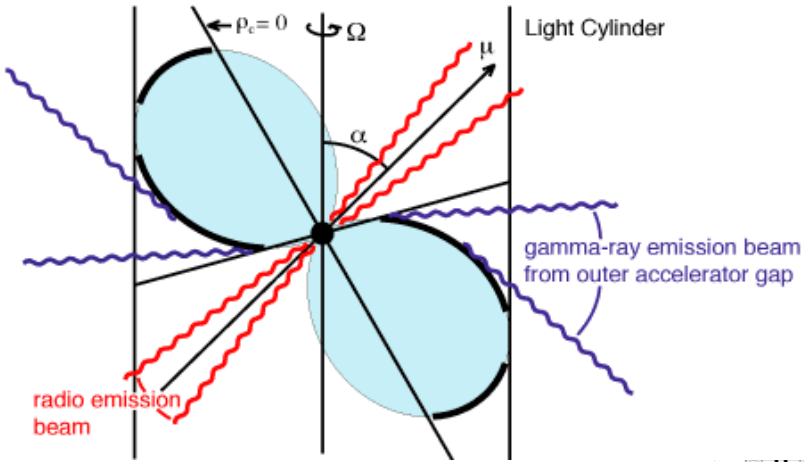


Credit: R.W. Romani

# Les modèles de structure magnétosphérique

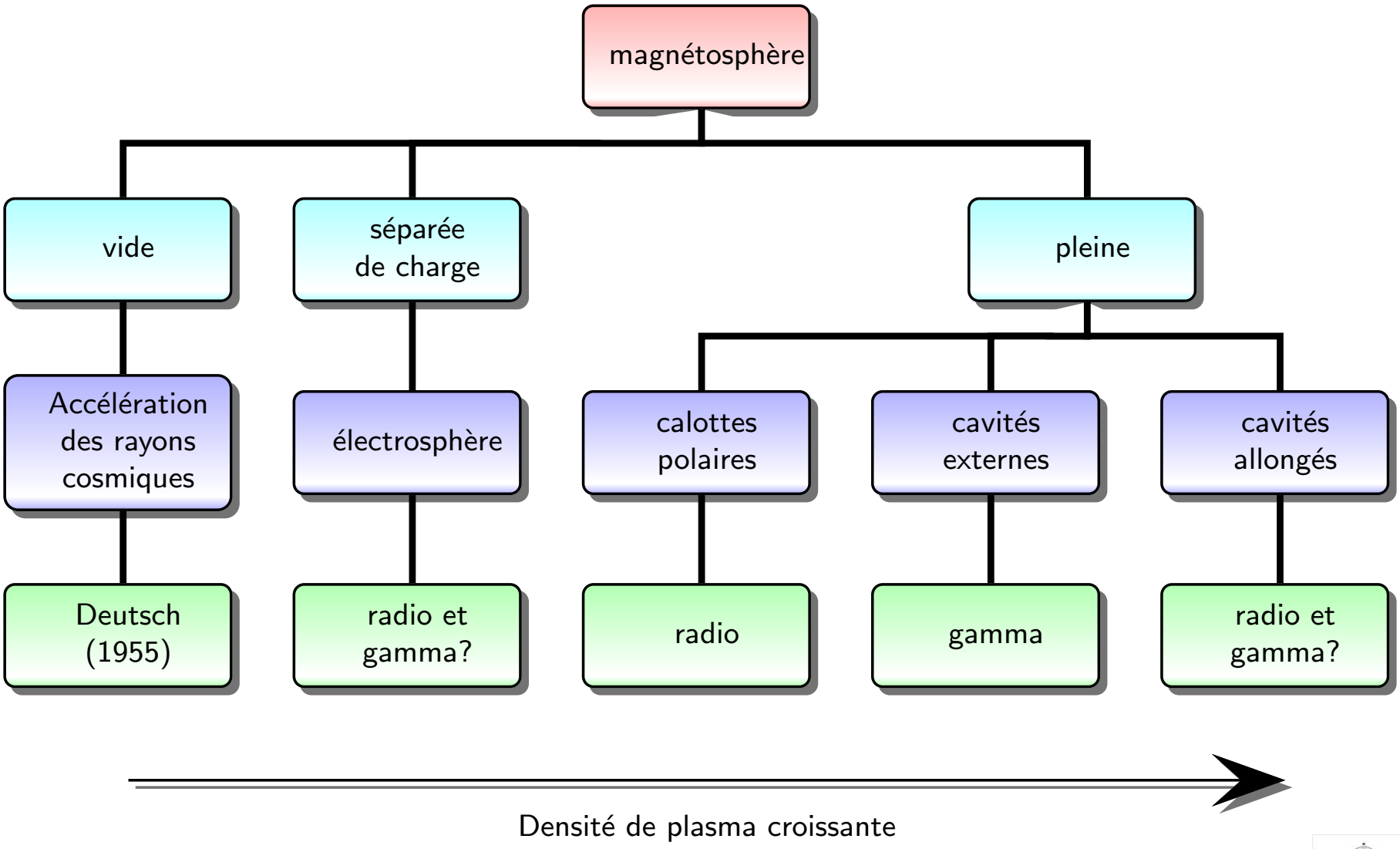


Figure: Vue synthétique des modèles de magnétosphère de pulsar. Les modèles peu denses sont situés à gauche tandis que les magnétosphères pleines et denses se situent à droite.

# Modèle phénoménologique pour l'émission radio

Interprétation des pulses radio: plusieurs composantes émettantes

- un cœur central
- un ou plusieurs cônes coaxiaux avec le cœur

$\Rightarrow$ classification de Rankin des pulses

Le modèle du vecteur tournant rend compte dans le domaine radio

- de l'évolution de la polarisation en fonction de la phase
- de la forme des pulses: simple, double, multiple

(Radhakrishnan & Cooke, ApL, 1969)

Hypothèses

- champ magnétique dipolaire
- rayonnement de courbure le long des lignes de champ polaires
- polarisation dans le plan de courbure, défini par l'axe de rotation et la ligne de champ
- angle de polarisation varie en forme de S comme observé

Modèle récemment mis en défaut pour une vingtaine de pulsars (Yan et al. MNRAS, 2011)

# Modèle phénoménologique pour l'émission radio

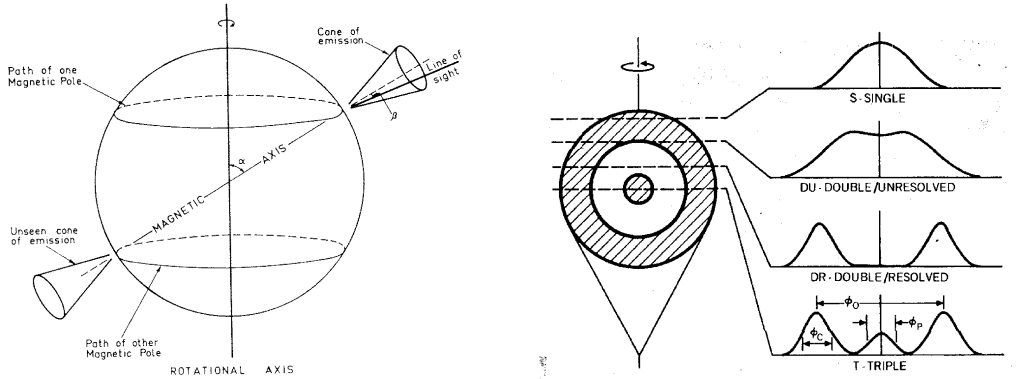


Figure: Schéma du modèle du cône creux (Radhakrishnan & Cooke, ApL, 1969).

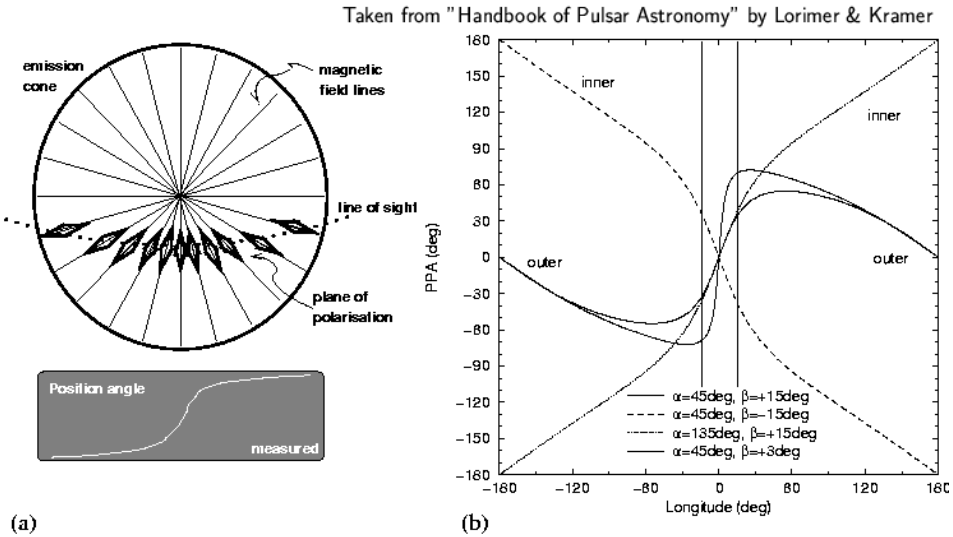


Figure: Modèle du vecteur tournant (Lorimer & Kramer).

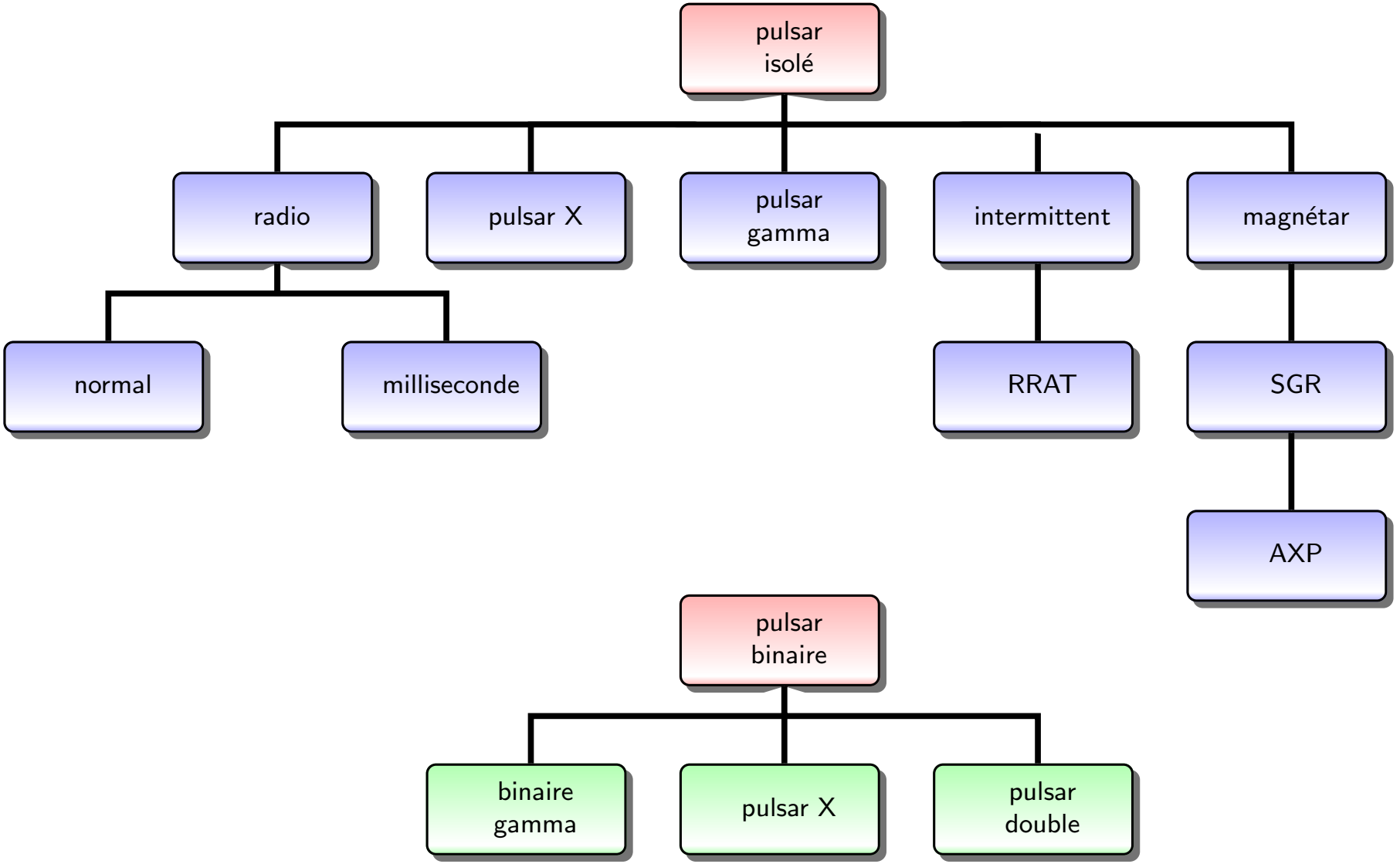
pulsar
isolé
radio
pulsar X
pulsar
gamma
intermittent
magnétar
normal
milliseconde
RRAT
SGR
AXP
pulsar
binaire
binaire
gamma
pulsar X
pulsar
double

# Supernova remnant and nebula

- the pulsar and its magnetosphere, source of *relativistic* $e^{\pm}$ *pairs*.

Figure: Link between the pulsar and its surrounding nebula.

# Supernova remnant and nebula

- the pulsar and its magnetosphere, source of *relativistic* $e^{\pm}$ *pairs*.
- the cold ultra-relativistic wind streaming to the nebula.

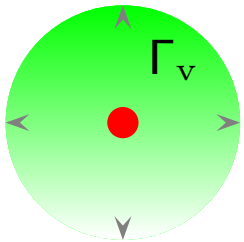


Figure: Link between the pulsar and its surrounding nebula.

# Supernova remnant and nebula

- the pulsar and its magnetosphere, source of *relativistic* $e^{\pm}$ *pairs*.
- the cold ultra-relativistic wind streaming to the nebula.
- the shocked wind composed of particles heated after crossing the *MHD shock* $\Rightarrow$ *main source of radiation* observed in radio, optics, X-rays and gamma-rays.

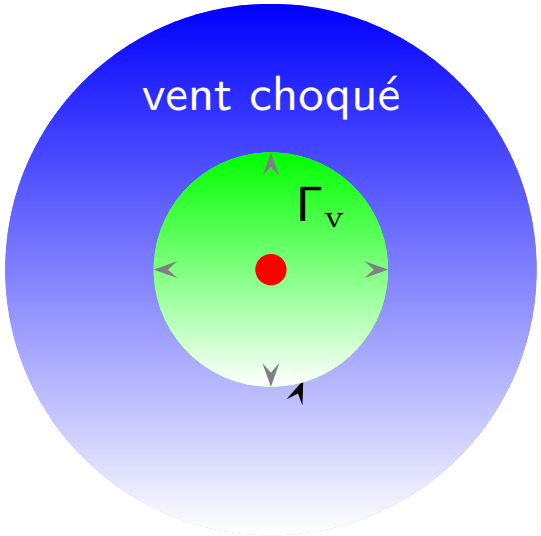


Figure: Link between the pulsar and its surrounding nebula.

# Supernova remnant and nebula

- the pulsar and its magnetosphere, source of *relativistic* $e^{\pm}$ *pairs*.
- the cold ultra-relativistic wind streaming to the nebula.
- the shocked wind composed of particles heated after crossing the *MHD shock* $\Rightarrow$ *main source of radiation* observed in radio, optics, X-rays and gamma-rays.
- the supernova remnant.

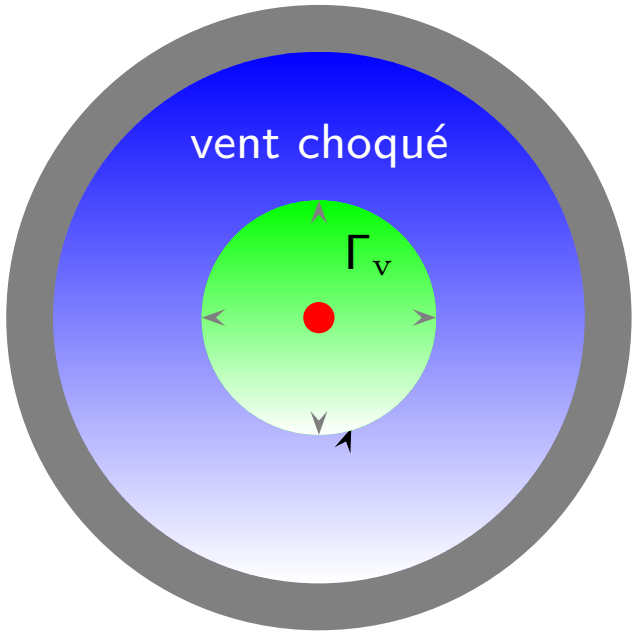


Figure: Link between the pulsar and its surrounding nebula.

# Supernova remnant and nebula

- the pulsar and its magnetosphere, source of *relativistic* $e^{\pm}$ *pairs*.
- the cold ultra-relativistic wind streaming to the nebula.
- the shocked wind composed of particles heated after crossing the *MHD shock* $\Rightarrow$ *main source of radiation* observed in radio, optics, X-rays and gamma-rays.
- the supernova remnant.
- the interstellar medium.

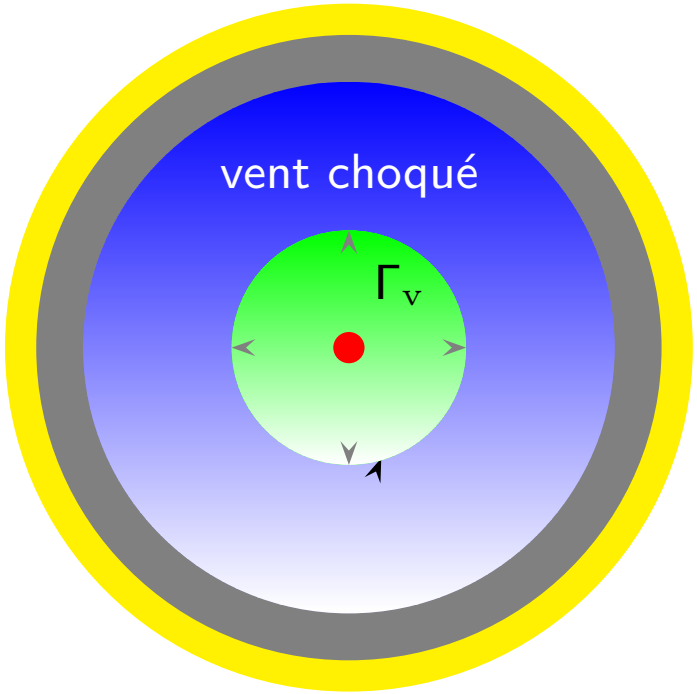


Figure: Link between the pulsar and its surrounding nebula.

# Magnetic field

- Faraday rotation of polarized emission from pulsars can map the magnetic field structure of the Milky Way.
- The rotation measure RM is

$$\mathrm{RM} = 0.81 \times 10^{-6} \int \left(\frac{n_\mathrm{e}}{1\ \mathrm{m}^{-3}}\right) \left(\frac{B_\parallel}{10^{-10}\ \mathrm{T}}\right) \left(\frac{dl}{1\ \mathrm{pc}}\right) \tag{5}$$

with $n_e$ the electron density number, $B_\parallel$ magnetic field component along the line of sight, $dl$ the distance traveled through the medium.

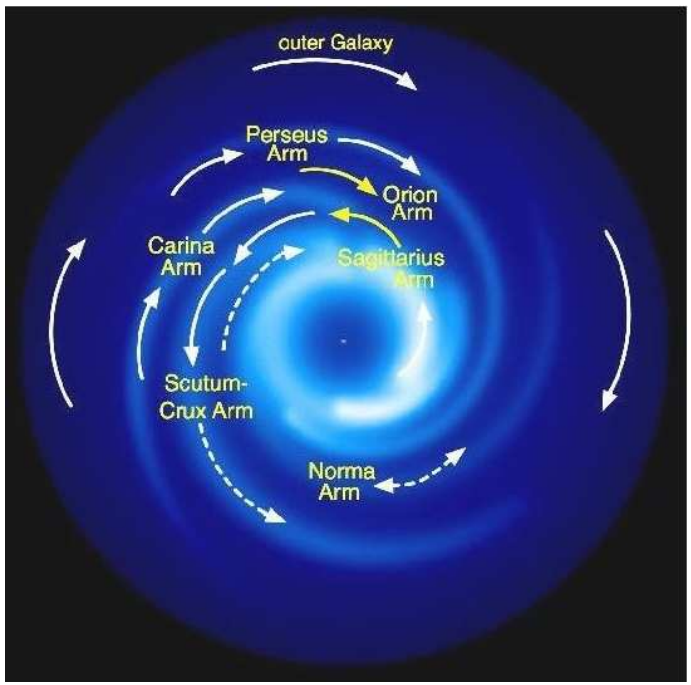


(from Jo-Anne Brown, Calgary)

- moreover from the dispersion measure DM, $\Rightarrow$ mean magnetic field along the line of sight $< B_\parallel >$.
- magnetic field estimate in the spiral arms $10^{-10}$ T.

# Planets around pulsars

- orbiting object around a pulsar can perturb the secular increase in pulsar period.

$\Rightarrow$ extrasolar planet detection.

- case of PSR B1257+12 with gravitational resonance of 3 : 2 kind between two planets $\Rightarrow$ strong evidence without doubt.
- Earth like planets become detectable (comparable masses $M_\oplus$).
- in 2003, second PSR B1620-26, geant planet with 2.5 $M_{\mathrm{J}}$ and a white dwarf companion $M_{\mathrm{nb}} \approx 0.34\, M_\odot$.

| PSR | Planète | Masse | Demi-grand axe | Période orbitale | Découverte |
|---|---|---|---|---|---|
| B1620-26 | PSR B1620-26 b | 2.5 $M_J$ | 23 UA | 100 ans | 2003 |
| B1257+12 | B1257+12 A | 0.020 $M_\oplus$ | 0.19 UA | 25.262 jours | 1994 |
| | B1257+12 B | 4.3 $M_\oplus$ | 0.36 UA | 66.5419 jours | 1992 |
| | B1257+12 C | 3.90 $M_\oplus$ | 0.46 UA | 98.2114 jours | 1992 |

Table: List of confirmed planets around pulsars.

# Gravitational waves: orders of magnitude

A central prediction of GR is the existence of GW. Unfortunately

- impossible to test relativistic gravity on Earth.
- in the solar system, only possible in weak fields.

But

- binary pulsars are good candidates to check general relativity and alternative theories of gravity.

Hope to see radiation from small perturbation $\varepsilon$ with respect to axisymmetry where $\varepsilon I$ represents the asymmetric part of the moment of inertia.

The gravitational luminosity is

$$L_{\mathrm{GW}} \approx \frac{c^5}{G} \varepsilon^2 \left(\frac{R_s}{R}\right)^2 \left(\frac{v}{c}\right)^6 \approx 10^{52}\ \mathrm{W}\, \varepsilon^2 \left(\frac{R_s}{R}\right)^2 \left(\frac{v}{c}\right)^6 \tag{6}$$

$\Rightarrow$ excellent candidates are

- compact objects, $R \sim R_s$.
- in rapid motion, $v \sim c$.
- significant aymmetry.

$\Rightarrow$ like neutron stars.

# Sources of gravitational waves

Luminosity can be high even for small perturbations. Unfortunately, spacetime is very rigid and viscous, high luminosity does not mean large amplitudes for oscillations. To the contrary, the relative amplitude of gravitational waves for a source at distance $d$ is only

$$h \approx 10^{-25} \left(\frac{\varepsilon}{10^{-6}}\right) \left(\frac{I_{zz}}{10^{38}\ \mathrm{kg\ m^2}}\right) \left(\frac{\nu}{100\ \mathrm{Hz}}\right)^2 \left(\frac{100\ \mathrm{pc}}{d}\right) \tag{7}$$

Neutrons stars are continuous sources of gravitational waves. Three main phenomena to generate them

- non axisymmetric perturbations of the star.
- unstable oscillations in the fluid (rotation modes $r$).
- precession.

Observed frequencies are around the neutron star spin frequency and expected amplitudes too weak for current detectors.

Accreting neutrons stars in X-ray binaries are a special class with rotation in the range [200,600] Hz, far from the limit of 1,4 kHz. Acceleration of the rotation by accretion of plasma must be braked by angular momentum loss, gravitational waves exerting a torque proportional to $\Omega^5$ furnishing an explanation of the clustering in a narrow $\Omega$ range.

# Pulsar timing of isolated pulsars

Pulsars are excellent clocks in the sky, very stable, comparable to atomic clocks.
But their true period differs from the measured one on Earth
$\Rightarrow$ needs to be corrected
$\Rightarrow$ pulsar timing.
The time of arrival (TOA) must take into account many effects that modify the arrival time of a photon on the telescope. The main effects are

- Earth is not an inertial frame thus topocentric clock time $t_{\rm topo}$ is not equal to solar system barycenter clock time $t_{\rm SSB}$ (our best approximate inertial frame).
- dispersion measure $< DM >$ contributing with a terme proportional to $\frac{<\rm DM>}{\nu^2}$.
- Rœmer delay $\Delta_{\rm R\odot}$.
- Shapiro delay $\Delta_{\rm S\odot}$.
- Einstein delay $\Delta_{\rm E\odot}$.

Summarizing all these contributions, we get

$$t_{\rm SSB} = t_{\rm topo} + {\rm cst}\,\frac{< DM >}{\nu^2} + \Delta_{\rm R\odot} + \Delta_{\rm E\odot} + \Delta_{\rm S\odot} \tag{8}$$

$\odot$ refers to effects related to the motion of Earth along its orbit around the Sun.

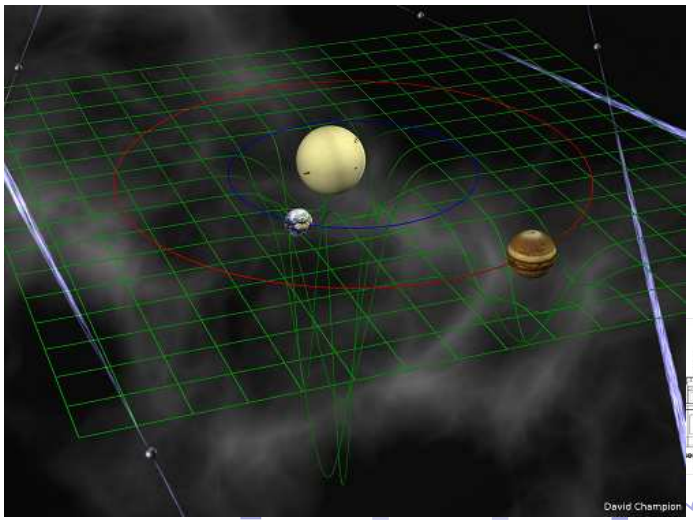

# Rœmer delay

Rœmer delay $\Delta_{\mathrm{R}\odot}$ is due to the light travel time in the solar system according to the motion of Earth around the Sun

$$\Delta_{\mathrm{R}\odot} = -\frac{\vec{n}\cdot\vec{r}}{c} \tag{9}$$

- $\vec{r}$ from the observer to the barycentre of the solar system.
- $\vec{n}$ the unit vector along the line of sight.
- $c$ the speed of light.

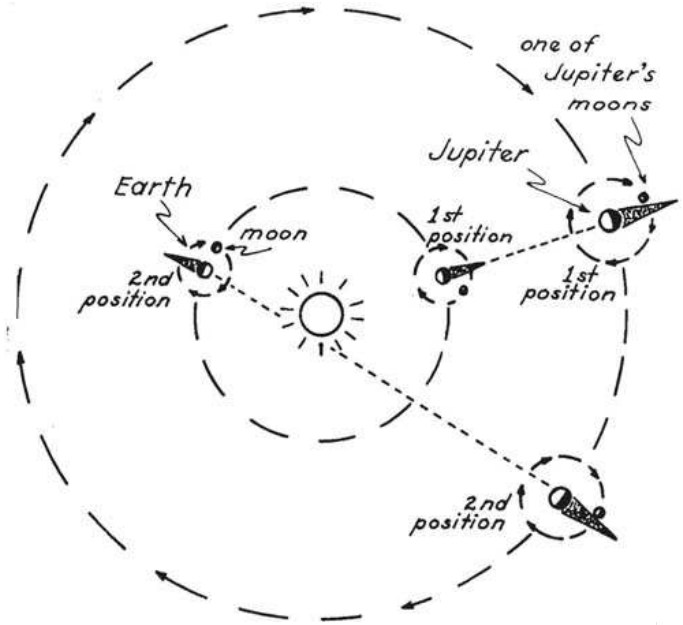

# Shapiro delay

Shapiro delay is due to curvature of spacetime, light need an extra delay to come to the obsever because the path is longer than in flat spacetime.

$$\Delta_{\mathrm{S}\odot} = -2 \sum_i \frac{G\, M_i}{c^3} \ln\left(\frac{\vec{n}\cdot\vec{r}_i^{\,E} + r_i^E}{\vec{n}\cdot\vec{r}_i^{\,P} + r_i^P}\right) \tag{10a}$$

$$\approx -\frac{2\, G\, M_\odot}{c^3} \ln(1+\cos\vartheta) \tag{10b}$$

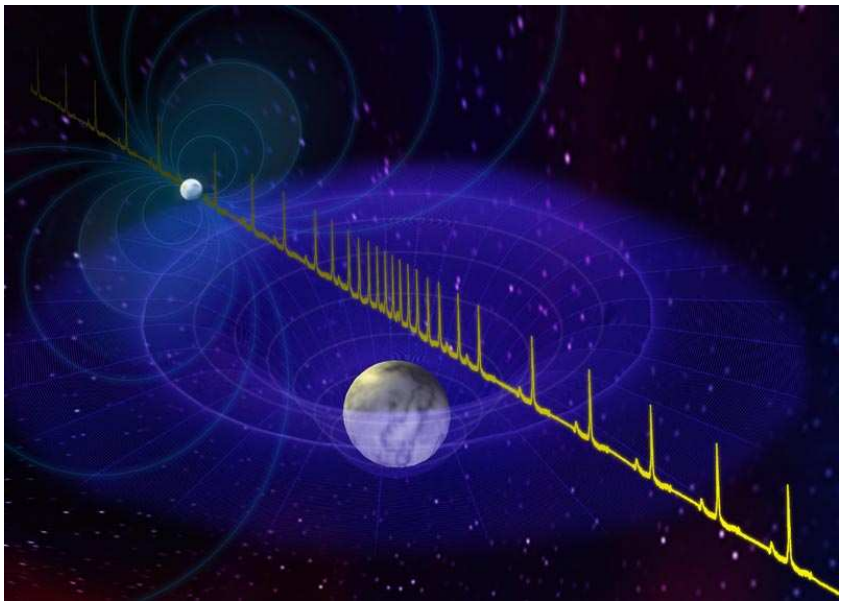

where

- $M_i$ mass of object $i$ (planet, Sun).
- $\vec{r}_i^{\,E}$ position of object $i$ with respect to Earth
- $\vartheta$ angle formed by the triangle pulsar-Sun-Earth.

# Einstein delay

A clock $\tau$ in a gravitational field ticks more slowly than one $t$ far away from gravitating bodies

$$d\tau = \sqrt{1 - \frac{R_s}{R}}\, dt \tag{11}$$

not to be confused with time dilation from relative motion.

On the surface of the Earth, for instance the difference is one part about $10^9$, a difference of 1 ns every second!

Einstein delay $\Delta_{\mathrm{E}}$ is caused by

- gravitational redshift effects.
- time dilation.

due to the motion of Earth in the gravitational potential of the solar system inducing a delay

$$\frac{d\Delta_{\mathrm{E}\odot}}{dt} = \sum_i \frac{G\, M_i}{c^2\, r_i^E} + \frac{v_E^2}{2\, c^2} - cste \tag{12}$$

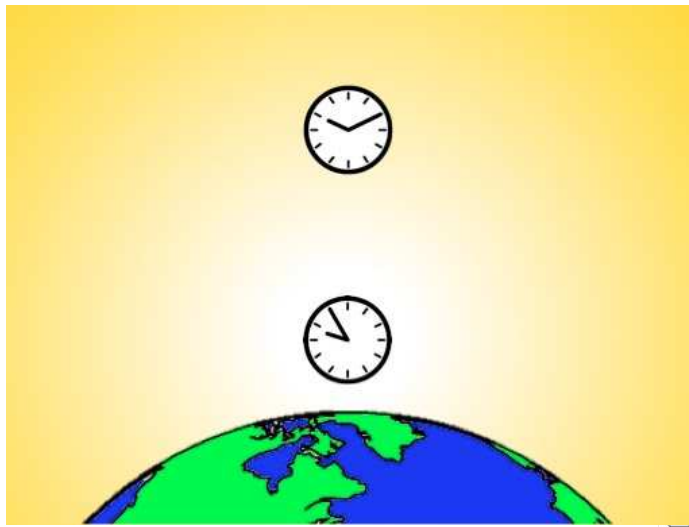

# What about binary systems: neutron stars binaries

- about 11 such systems known (DNS).
- separation between the two components $\gg$ radius of the star

$\Rightarrow$ compact object considered as a point mass

$\Rightarrow$ no tidal effect

$\Rightarrow$ neither mass transfert.

$\Rightarrow$ very clean systems.

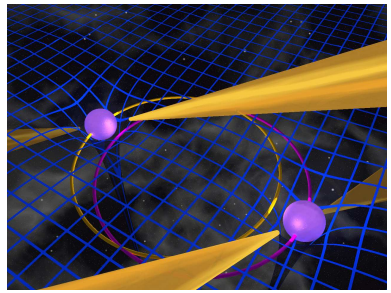

| | P(ms) | $P_b$(d) | x(lt-s) | e | $P_{\rm geo}$(deg/yr) |
|---|---|---|---|---|---|
| J0737-3039 | 22.7/2770 | 0.10 | 1.42/1.51 | 0.09 | 4.8/5.1 |
| B1534+12 | 37.9 | 0.42 | 3.73 | 0.27 | 0.5 |
| J1518+4904 | 40.9 | 8.64 | 20.0 | 0.25 | - |
| J1756-2251 | 28.5 | 0.32 | 2.76 | 0.18 | 0.76 |
| J1753-2240 | 95.1 | 13.63 | 18.1 | 0.30 | - |
| J1811-1736 | 104.2 | 18.8 | 34.8 | 0.83 | - |
| J1829+2456 | 41.0 | 1.18 | 7.24 | 0.14 | 0.08 |
| J1906+0746 | 144.1 | 0.17 | 1.42 | 0.09 | 2.2 |
| B1913+16 | 59.0 | 0.33 | 2.34 | 0.62 | 1.2 |
| B2127+11C | 30.5 | 0.34 | 2.52 | 0.68 | 1.9 |

# neutron star/white dwarf binaries

- relativistic effects less important but some interesting aspects.
- check of the strong equivalence principle (SEP) = free fall state independent of the internal gravitational energy of the object, weak deviation $\Delta < 0.009$ could exist.
- violation of SEP.

$\Rightarrow$ Nordtvedt effect = two objects fall differently in the same external gravitational field.

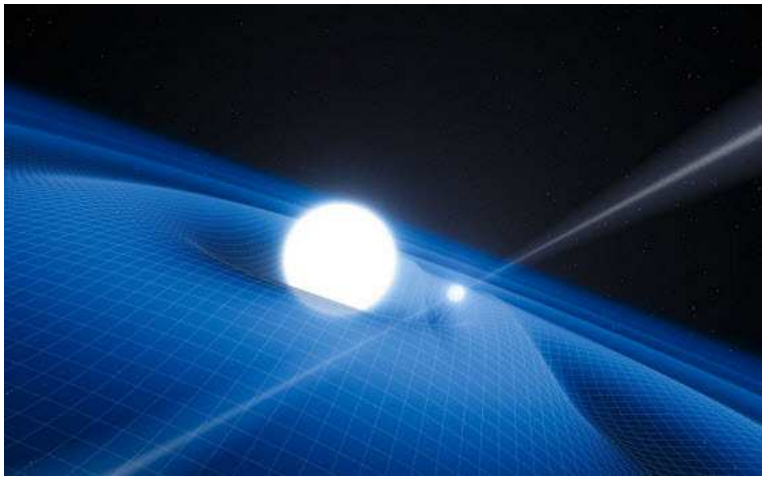

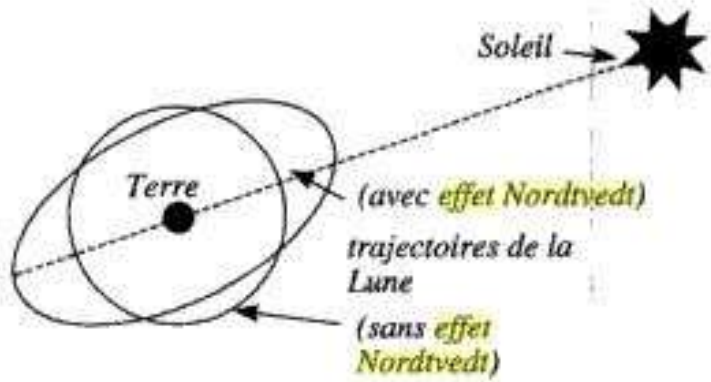

# Keplerian orbital parameters

In the classical keplerian description, the 5 orbital parameters are

1. projection of semi-major axis $a$.
2. eccentricity $e$.
3. binary period $P_{\rm b}$.
4. longitude of periastron $\omega$.
5. time of passage through periastron $T_0$.

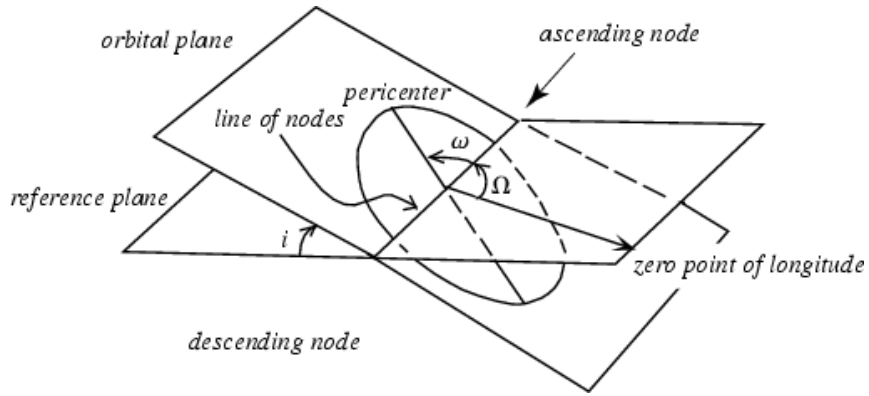

# Relativistic binary timing

The time of arrival (TOA) must take into account many effects that modify the arrival time of a photon on the telescope. The main effects are

- Rœmer delay $\Delta_{\rm RB}$.
- Shapiro delay $\Delta_{\rm SB}$.
- Einstein delay $\Delta_{\rm EB}$.

but now associated to the orbital motion of the neutron star, not Earth motion.

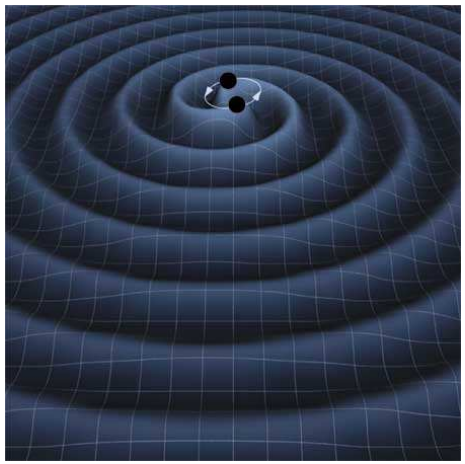

(T. Carnahan (NASA GSFC))

Summarizing all the contributions, we get

$$t_{\rm SSB} = t_{\rm topo} + {\rm cst}\,\frac{< DM >}{\nu^2} + \Delta_{\rm R\odot} + \Delta_{\rm E\odot} + \Delta_{\rm S\odot} + \Delta_{\rm RB} + \Delta_{\rm EB} + \Delta_{\rm SB} \qquad (13)$$

- $\odot$ refers to the motion of Earth along its orbit around the Sun.
- $B$ corresponds to the motion in the binary orbit.

# Rœmer delay

Rœmer delay $\Delta_{\mathrm{RB}}$ is caused by the orbital motion of the pulsar.

It includes

- acceleration effects
  - Shklovsky.
  - transverse Doppler.
- relativistic deformation of the orbit, parameterized by $e_r$ and $e_\vartheta$.

$$\Delta_{\mathrm{RB}} = x\,(\cos E - e_r)\,\sin\omega + x\,\sin E\,\sqrt{1-e_\vartheta^2}\,\cos\omega \tag{14}$$

$E$ is the anomalous eccentricity.

# Shapiro delay

Shapiro delay for a binary becomes

$$\Delta_{\rm SB} = -2\,r\,\ln\left[1 - e\,\cos E - s\left(\sin\omega\left(\cos E - e\right) + \sqrt{1-e^2}\cos\omega\,\sin E\right)\right] \tag{15}$$

and for small eccentricities

$$\Delta_{\rm SB} \approx -2\,r\,\ln\left[1 - s\,\sin\Phi\right] \tag{16}$$

where $\Phi$ orbital phase.

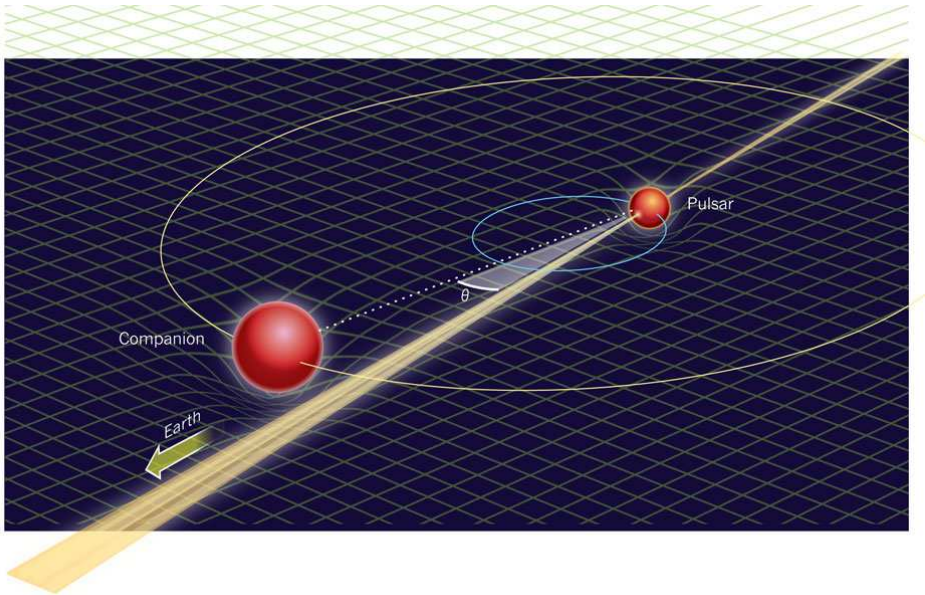


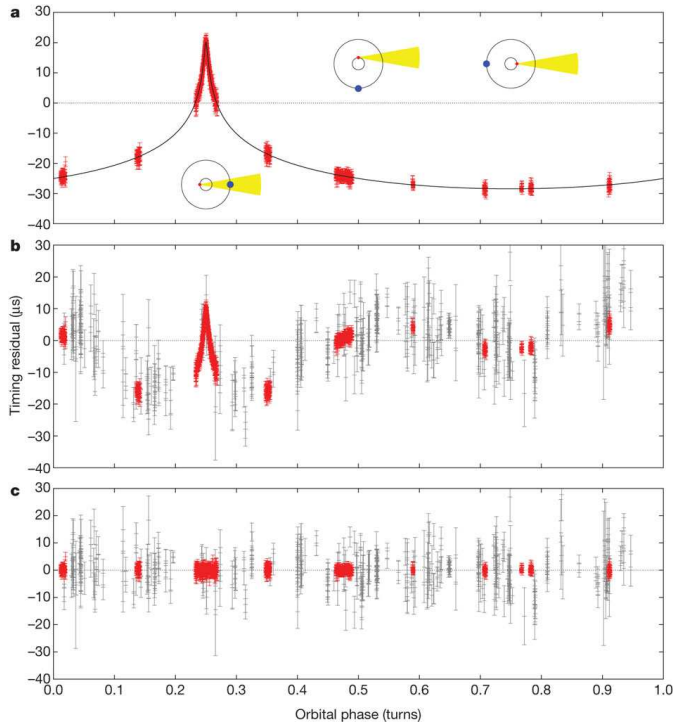


(Demorest et al., Nature, 2010)

# Einstein delay

- gravitational redshift largest when pulsar closest to the companion
  $\Rightarrow$ happens at periastron.
- but then also orbital speed largest, thus special relativistic time dilation effect important.

The relativistic time delay is the difference between what is observed and what would be measured if the pulsar were in a circular orbit, i.e. at constant distance and with constant speed around its companion
$\Rightarrow$ no variation in time dilation and gravitational redshift.

$$\Delta_{\rm EB} = \gamma \, sinE \qquad (17)$$

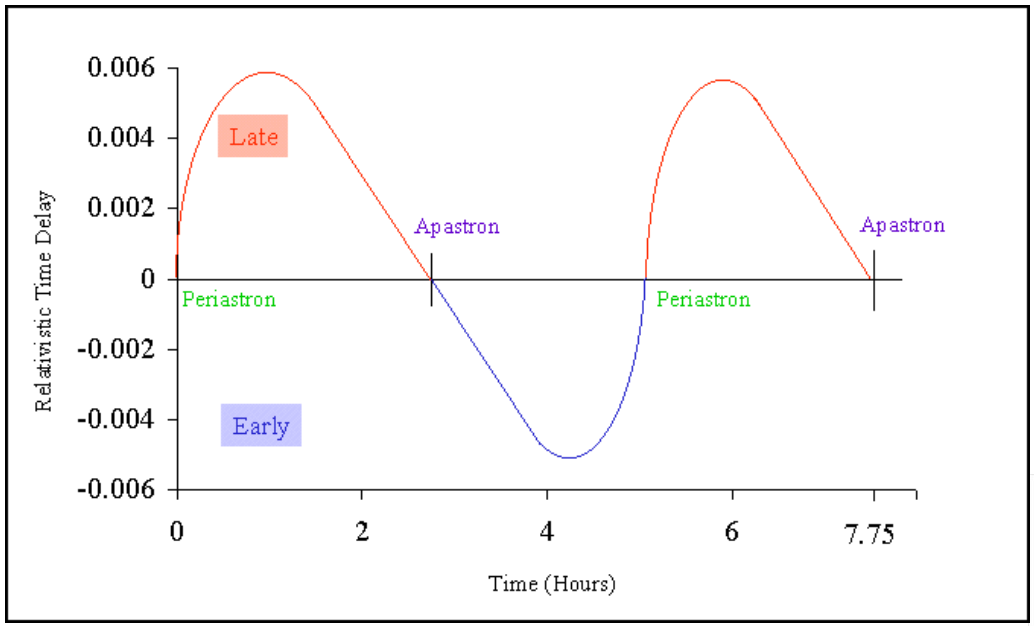

# Post-Keplerian orbital parameters

In general relativity, there is no exact solution to the two body-problem.
$\Rightarrow$ look for the change in the keplerian parameters.
$\Rightarrow$ compute post-Keplerian orbital parameters.

Relativistic motion in binary systems affects the TOA, corrections are symbolized by 5 post-Keplerian orbital parameters

1. orbital decay $\dot{P}_{\rm b}$ induced by gravitational wave emission.
2. relativistic advance of perihely $\dot{\omega}$.
3. Einstein parameter or relativistic factor $\gamma$ related to $\Delta_{\rm EB} = \gamma \sin E$.
4. range $r$ and shape $s$ of Shapiro delay $\Delta_{\rm SB} = -2\, r\, \ln(1 - s \sin \Phi)$ with $\Phi$ orbital phase $s = \sin i$, $i$ inclination of the orbit.

$\Rightarrow$ Note that all these post-keplerian parameters are determined by the 5 keplerian parameters.

# Post-Keplerian orbital parameters

If Einstein theory of gravity is correct, then

$$\dot{\omega}_{\rm b} = 3 \left( \frac{P_{\rm b}}{2\,\pi} \right)^{-5/3} T_{\odot}^{2/3} \, \frac{(m_{\rm p} + m_{\rm c})^{2/3}}{1 - e^2} \tag{18a}$$

$$\gamma = \left( \frac{P_{\rm b}}{2\,\pi} \right)^{1/3} T_{\odot}^{2/3} \, e \, \frac{m_{\rm c}\,(m_{\rm p} + 2\,m_{\rm c})}{(m_{\rm p} + m_{\rm c})^{4/3}} \tag{18b}$$

$$\dot{P}_{\rm b} = -\frac{192\,\pi}{5} \left( \frac{P_{\rm b}}{2\,\pi} \right)^{-5/3} T_{\odot}^{5/3} \left( 1 + \frac{73}{24}\,e^2 + \frac{37}{96}\,e^4 \right) \frac{m_{\rm p}\,m_{\rm c}}{(m_{\rm p} + m_{\rm c})^{1/3}\,(1 - e^2)^{7/2}} \tag{18c}$$

$$r = T_{\odot}\,m_{\rm c} \tag{18d}$$

$$s = x \left( \frac{P_{\rm b}}{2\,\pi} \right)^{-2/3} T_{\odot}^{-1/3} \, \frac{(m_{\rm p} + m_{\rm c})^{2/3}}{m_{\rm c}} \tag{18e}$$

where

$$T_{\odot} = \frac{G\,M_{\odot}}{c^3} \approx 4.925\ \mu s \tag{19}$$

Note that

- there are only two unknowns, the masses $(m_p, m_c)$.
- known orbital parameters $(P_b, x = a \sin i, e)$.

# Post-Keplerian orbital parameters: test of gravity

How can we then test alternative theories of gravity?

For instance, for GR

- post-keplerian (PK) parameters are described by the mass of the pulsar $m_p$ and its companion $m_c$ only.
- knowing 2 PK parameters we deduce the masses of both stars.
- any other PK parameter gives a check of the self-consistency of the theory.
- $n$ PK give $n$ curves in the $(m_p, m_c)$ plane, all must pass through a same point.

$\Rightarrow$ $(n-2)$ tests of a theory of gravity.

In some special binaries, even more PK parameters are measurable (see later)

- geodetic precession observed.
- mass ratio constrained $R = m_p/m_c$.

# Coalescence time for binary neutron stars

From the orbital decay, we can guess the time for coalescence of a binary by

$$T_c = \frac{5}{256}\,\frac{a^4\,c^5}{G^3\,m_{\rm p}\,m_{\rm c}\,(m_{\rm p}+m_{\rm c})}\,(1-e^2)^{7/2}\,\left(1+\frac{73}{24}\,e^2+\frac{37}{96}\,e^4\right)^{-1} \tag{20}$$

For a quasi-circular orbit and stars of comparable masses, like neutron stars, null eccentricity $e = 0$ and $m_{\rm p} = m_{\rm c} = M$ so

$$T_c = \frac{5}{512}\,\frac{a^4\,c^5}{G^3\,M^3} \tag{21}$$

Typical coalescence time

- for PSR B1913+16, a few hundreds of millions years.
- for PSR J0737-3039, a few tenth of millions years

# The binary pulsar PSR B1913+16

| Quantité | Valeur |
|---|---|
| Période orbitale $P_{\rm b}$ | 0.322997462727(5) jo |
| Excentricité $e$ | 0.6171338(4) |
| Projection demi-grand axe (s) | 2.341774(1) |
| Longitude périastre $\omega$ (deg) | 226.57518(4) |
| Avance du périhélie $\dot{\omega}$ | 4.226607(7) deg/an |
| $\dot{P}_{\rm b}$ (prédiction) | $-2.402 \times 10^{-12}$ |
| $\dot{P}_{\rm b}$ (observée) | $-2.4211(14) \times 10^{-12}$ |
| Décalage gravitationnel $\gamma$ | 4.294(1) |
| Orbit decay | 1 cm/day |

Table: Quelques paramètres képlériens et post-képlériens du pulsar binaire PSR 1913+16.

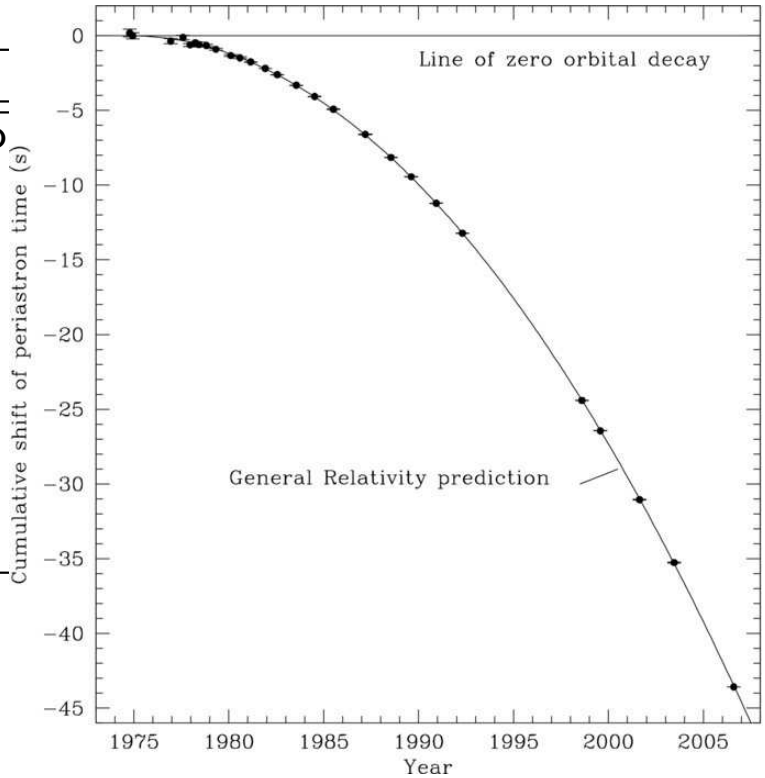


(Weisberg et al, ApJ, 2010)

# The double pulsar PSR J0737-3039

| | PSR J0737-3039A | PSR J0737-3039B |
|---|---|---|
| Période $P$ (ms) | 22.69937855615 | 2773.4607474 |
| Dérivée de la période $\dot{P}$ | $1.74 \times 10^{-18}$ | $0.88 \times 10^{-15}$ |
| Ascension droite (J2000) | 07h37m51s.247 | - |
| Déclinaison (J2000) | $-30^o39'40''.74$ | - |
| Mesure de dispersion DM (cm-3 pc) | 48.9 | 48.7 |
| Période orbitale $P_{\rm b}$ (jour) | 0.102251563 (1) | - |
| Excentricité $e$ | 0.087779 | - |
| Passage au périastre (MJD) | 52870.0120589 | - |
| Longitude du périastre $\omega$ (deg) | 73.805 | 73.805 + 180.0 |
| Projection du demi-grand axe $x = a(\sin i)/c$ (s) | 1.41504 | 1.513 |
| Avance du périaste (degree/an) | 16.90 (1) | - |
| Décalage gravitationnel $\gamma$ (ms) | 0.38 (5) | |
| Flux à 1390 MHz (mJy) | 1.6 (3) | 0-1.3 (3) |
| Âge caractéristique $\tau_{\rm c}$ (My) | 210 | 50 |
| Champ magnétique de surface (Gauss) | $6.3 \times 10^9$ | $1.2 \times 10^{12}$ |
| Luminosité rotationnelle $\dot{E}$ (erg/s) 6000 x 1030 | 2 x 1030 | |
| Fonction de masse ($M_\odot$) | 0.29097 (1) | 0.356 (3) |
| Distance (kpc) | 0.6 | |
| Masse totale du système $m_A + m_B$ ($M_\odot$) | 2.588 (3) | |
| Rapport de masse $R \equiv m_A/m_B$ | 1.069 (6) | |
| Masse ($M_\odot$) | 1.337 (5) | 1.250 (5) |

Table: Quelques propriétés du pulsar double.

# The double pulsar PSR J0737-3039

Because the orbit of both pulsars are known there is one more constraint given by the mass ratio

$$R \equiv \frac{m_A}{m_B} = \frac{a_B}{a_A} = \frac{x_B}{x_A} \qquad (22)$$

(Kramer et al., 2006)

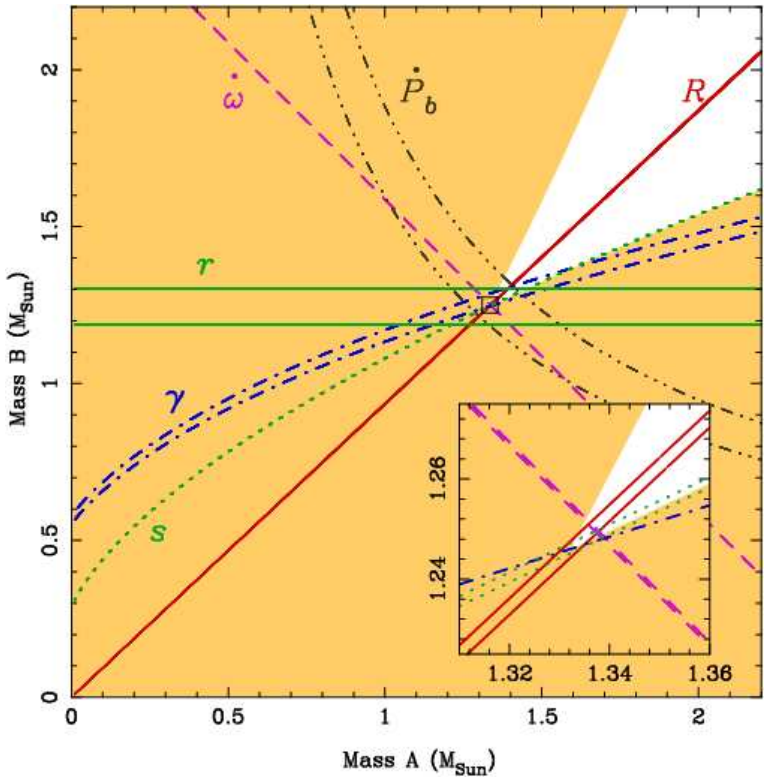


| PK parameter | Observed | GR expectation | Ratio |
|---|---|---|---|
| $\dot{\omega}$ (deg/yr) | 16.899 47(68) | - | - |
| $\dot{P}_b$ | 1.252(17) | 1.24787(13) | 1.003(14) |
| $\gamma_A$ (ms) | 0.3856(26) | 0.38418(22) | 1.0036(68) |
| $s$ | 0.999 74(-39, +16) | 0.999 87(-48, +13) | 0.999 87(50) |
| $r_A$ ($\mu$s) | 6.21(33) | 6.153(26) | 1.009(55) |
| $\Omega_{SO,B}$ (deg/yr) | 4.77(+0.66, -0.65) | 5.0734(7) | 0.94(13) |

(from Kramer & Wex, Class. & Quant. Grav., 2009)

# Geodetic precession

Spacetime curvature induces a precession of the reference frame of freely falling bodies.

For a gyroscope orbiting a massive body

$$\vec{\Omega}_{\rm geod} = -\frac{3\,G\,M}{2\,r^2\,c^2}\,\vec{v}\wedge\vec{e}_r \qquad (23)$$

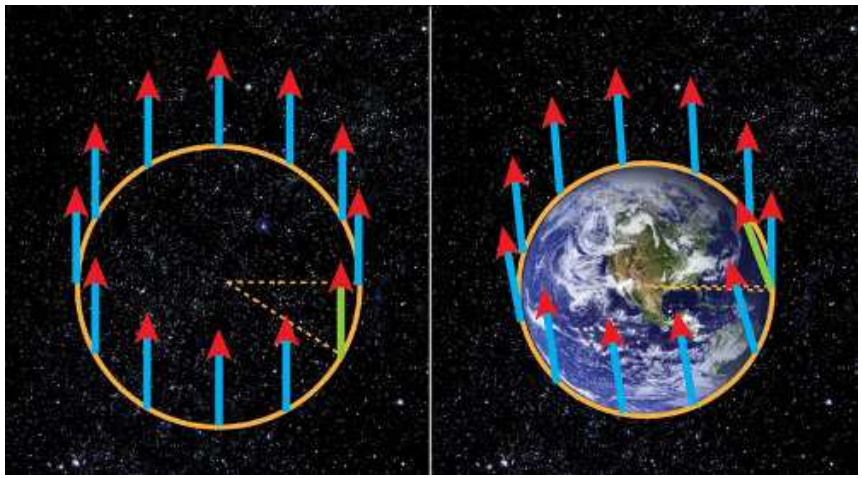

More specifically, for spinning neutron stars it leads to spin-orbit coupling through precession around the total angular momentum of the system $\approx$ orbital angular momentum of the binary $\vec{L}$ such that

$$\Omega_{\rm geod} = \left(\frac{2\,\pi}{P_b}\right)^{5/3} T_\odot^{2/3}\,\frac{1}{1-e^2}\,\frac{m_c\,(4\,m_p+3\,m_c)}{2\,(m_p+m_c)^{4/3}} \qquad (24)$$

most effective when $\vec{\Omega}$ and $\vec{L}$ are misaligned.

# Geodetic precession around Earth

Gravity Probe B results confirm the GR predictions of

- geodetic precession

$$\vec{\Omega}_{\rm geod} = -\frac{3\,G\,M}{2\,r^2\,c^2}\,\vec{v}\wedge\vec{e}_r \qquad (25)$$

- frame dragging (Lense-Thirring effect)

$$\vec{\Omega}_{\rm LT} = \frac{2\,G\,\vec{J}}{c^2\,a^3\,(1-e^2)^{3/2}} \qquad (26)$$

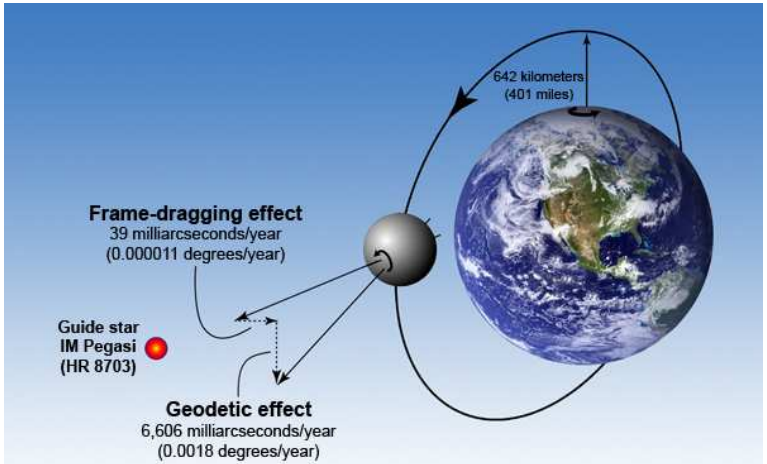


| | Measured | Predicted |
|---|---|---|
| Geodetic precession (mas) | 6602 ± 18 | 6606 |
| Frame-dragging (mas) | 37.2 ± 7.2 | 39.2 |

# Geodetic precession of the double pulsar

- geodetic precession of PSR J0737-3039 observed by the eclipsing phenomenon.
- magnetosphere of PSR B absorbes radiation from PSR A.
- model gives $\Omega_{so} \approx 4.77$ deg/yr.

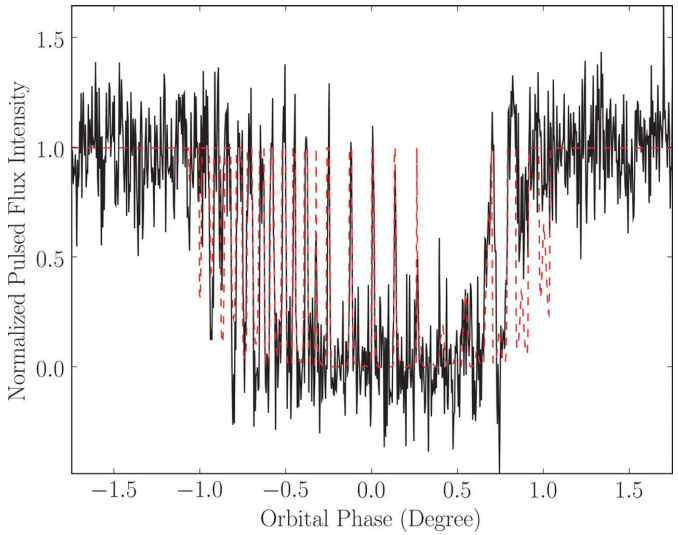


(Breton et al., Science 2008)

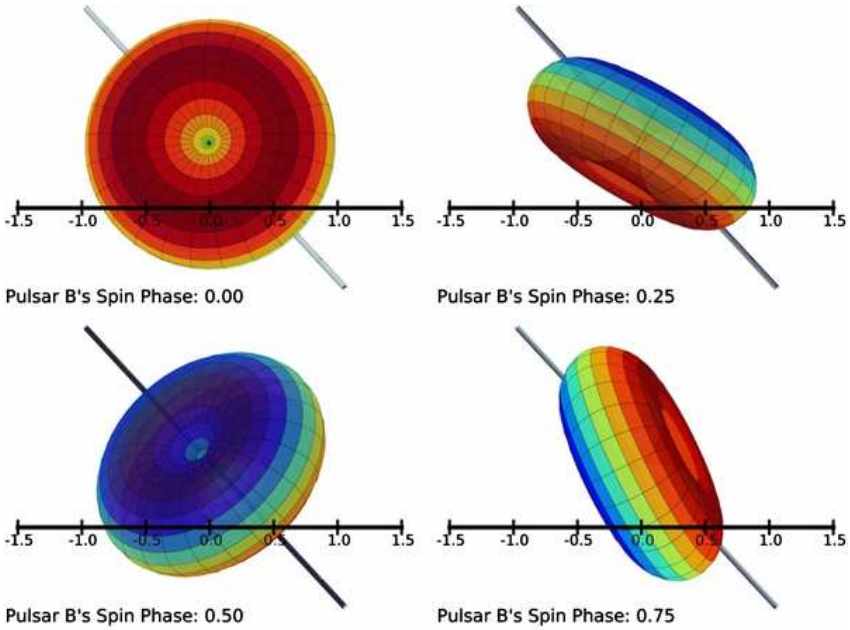


(Breton et al., ApJ 2012)

$\Rightarrow$ indirect proof of the dipolar structure of the pulsar magnetosphere!

# Geodetic precession applied to the double pulsar

geodetic precession of 75/71 years for PSR J0737-3039 A and B respectively

- ⇒ change in the orientation of the line of sight (spin-orbit coupling).
- ⇒ modification of the radio pulse profiles seen in PSR B but not in PSR A (unfavorable geometry, $\vec{\Omega} \parallel \vec{L}$).
- ⇒ constraint on the moment of inertia.
- ⇒ constraint on EOS, dense matter.

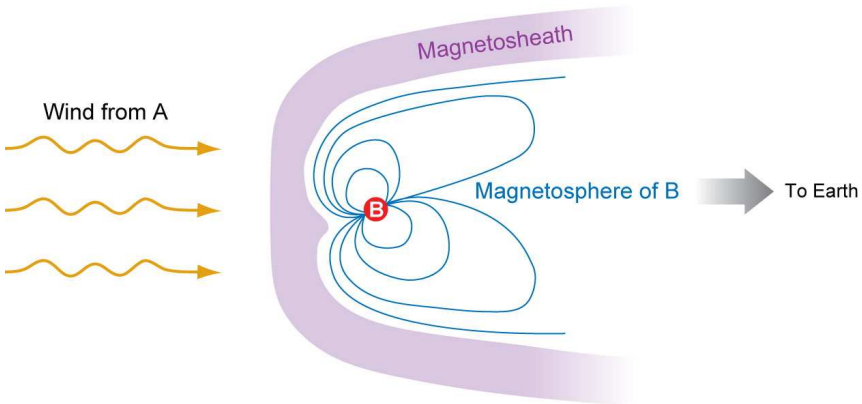


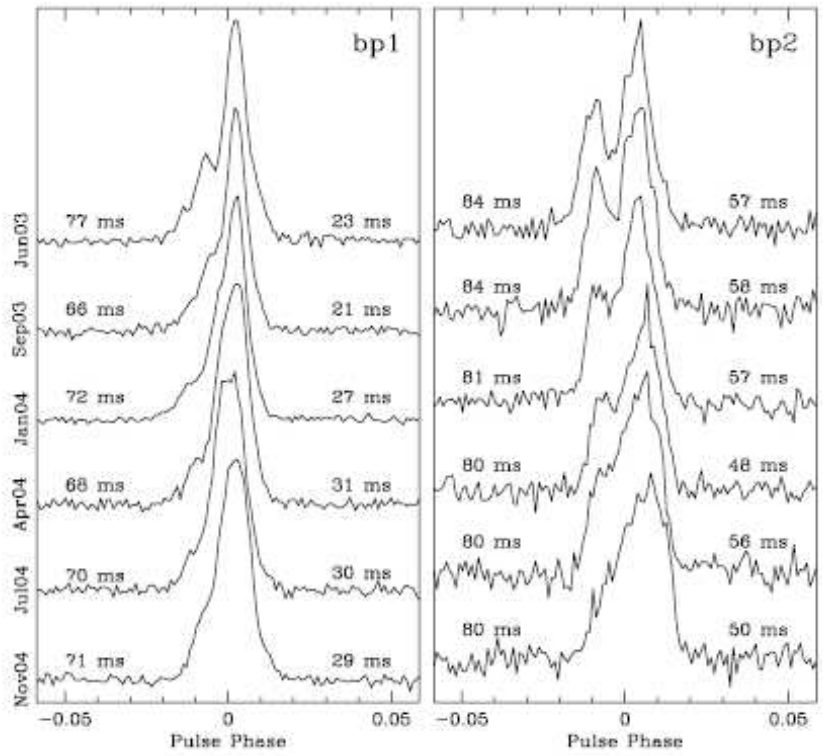


(Burgay et al, ApJ, 2005)

Kramer M, Stairs IH. 2008.
Annu. Rev. Astron. Astrophys. 46:541–72

# The future: Pulsar Timing Arrays

Pulsars are able to survey gravitational waves by measuring the modification of TOA. These perturbations induce an apparent change in the period of rotation
$\Rightarrow$ looking (again) for timing residual in pulsar timing.
$\Rightarrow$ use arrays of pulsars (PTA) like E(uropean)PTA and P(arkes)PTA.

- ms pulsars are best targets, because very stable clocks (low $\dot{P}$).
- detection of gravitational waves
  - from coalescence of BHs (nHz-$\mu$Hz).
  - from stochastic background predicted by some cosmology theories (nHz).
- sensitive to low frequencies
  $\Rightarrow$ complementarity to terrestrial instruments: LIGO, VIRGO, GEO600.

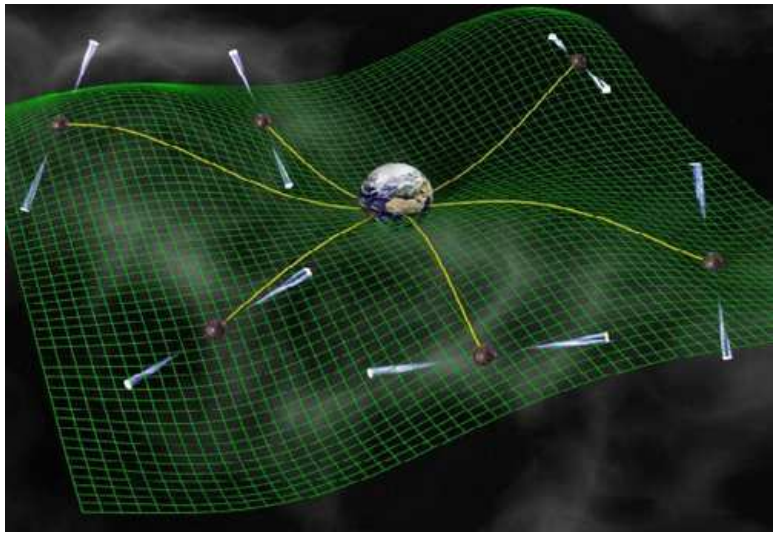

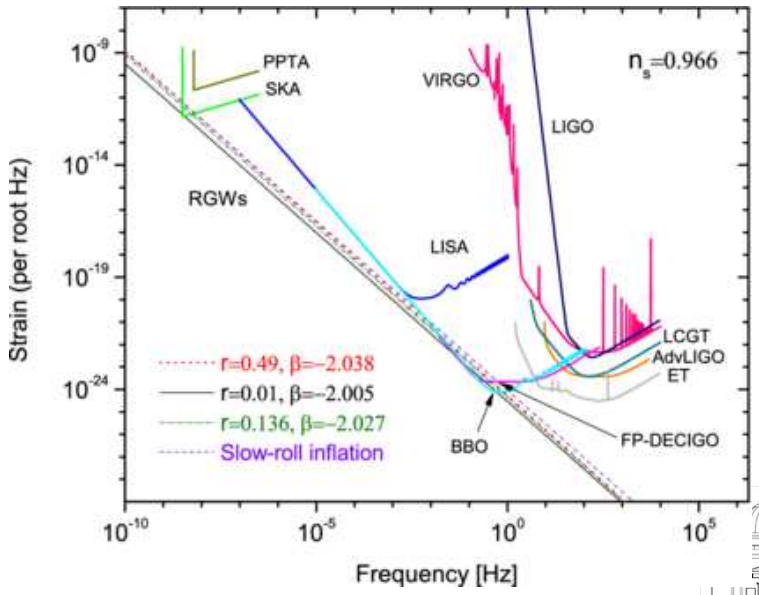


(Tong, Class. & Quant. Grav., 2012)

# Conclusions

## Broadband electromagnetic pulsed emission

- pulsars are observed from the radio wavelength up to HE/VHE (GeV/TeV) but explanation probably different for both extremes.
- not yet a clear picture of the magnetosphere and wind $\Rightarrow$ how do particle accelerate.
- radio polarisation constrains the geometry of the system.

## Very stabe clocks

- even if we do not understand how pulsars work, it is possible to use them as a very stable clock to diagnose plasma in the galaxy and test theories of gravity.
- pulsar timing very powerful in many areas of astrophysics.
- strong constrains on alternative theories of gravity, confirmation of gravitational wave but also some other post-newtonian effects (frame-dragging, geodetic precession) to good precision.

# Bibliography


- Pulsar Astronomy, A. Lyne & F. Graham-Smith, Cambridge University Press, 2006.
- Handbook of Pulsar Astronomy, D. Lorimer & M. Kramer, Cambridge University Press, 2004.
- Theory of Neutron Star Magnetospheres, F.C. Michel, University of Chicago Press, 1991.
- Physics of the Pulsar Magnetosphere, A.V. Gurevich, V.S. Beskin & Ya.N. Istomin, Cambridge University Press, 2006.
- Rotation and Accretion Powered Pulsars, Pranab Ghosh, World Scientific Publishing Company, 2007.
- Will C., The Confrontation between General Relativity and Experiment, Living Rev. Relativity 9 (2006), 3